Structure and evolution of Alanine/Serine Decarboxylases and the engineering of theanine production

Hao Wang[a,1], Biying Zhu[b,1], Siming Qiao[b], Chunxia Dong[b], Xiaochun Wan[b], Weimin Gong[a,*], Zhaoliang Zhang[b,*]

[a]Department of Life Sciences and Medicine, University of Science and Technology of China, Hefei, China.

[b]State Key Laboratory of Tea Plant Biology and Utilization, Anhui Agricultural University, Hefei, Anhui 230036, China.

[1]These authors contributed equally to this work.

* To whom correspondence should be addressed. Email: zhlzhang@ahau.edu.cn or wgong@ustc.edu.cn.

Author contributions: W.G, Z.Z and X.W designed research; H.W, B.Z, S.Q and C.D performed research; H.W and B.Z analyzed data; H.W, B.Z, W.G, and Z.Z wrote the paper.

Competing interest statement: The authors declare no competing financial interests.

Classification: Biochemistry (major), Plant Sciences (minor)

Keywords: alanine decarboxylase, serine decarboxylase, substrate specificity, theanine, *Camellia sinensis*

Abstract

Ethylamine (EA), the precursor of theanine biosynthesis, is synthesized from alanine decarboxylation by Alanine Decarboxylase (AlaDC) in tea plants. AlaDC evolves from Serine Decarboxylase (SerDC) through neofunctionalization and has lower catalytic activity. However, lacking structure information hinders the understanding of the evolution of substrate specificity and catalytic activity. In this study, we solved the X-ray crystal structures of AlaDC from *Camellia sinensis* (CsAlaDC) and SerDC from *Arabidopsis thaliana* (AtSerDC). Tyr^{341} of AtSerDC or the corresponding Tyr^{336} of CsAlaDC is essential for their enzymatic activity. Tyr^{111} of AtSerDC and the corresponding Phe^{106} of CsAlaDC determine their substrate specificity. Both CsAlaDC and AtSerDC have a distinctive zinc finger that contributes to the activity and has not been identified in any other Group II PLP-dependent amino acid decarboxylases. Based on the structure comparison and evolution analysis AlaDC or SerDC led us to perform mutation screen of CsAlaDC. The results indicated that the mutation of L110F or P114A in the CsAlaDC dimerization interface significantly improved the catalytic activity by 110% and 59%, respectively. Combining double mutant $CsAlaDC^{L110F/P114A}$ with theanine synthetase increased 672% of theanine production in an *in vitro* system. This study provides the structural basis for the substrate selectivity and catalytic activity of CsAlaDC and AtSerDC and sheds light on a new direction for the efficient industrial synthesis of theanine.

Introduction

Tea is one of the most popular natural non-alcoholic beverages consumed worldwide. About 2 billion cups of tea are consumed worldwide daily (1). The popularity of tea is determined by its favorable flavor and numerous health benefits (2-4). The flavor and health-beneficial effects of tea are conferred by the abundant secondary metabolites, including catechins, caffeine, theanine, volatiles, etc (5). Theanine (γ-glutamylethylamide) is a unique non-protein amino acid and the most abundant free amino acid in tea plants (*Camellia sinensis*). It accounts for more than 50% of the total free amino acids and approximately 1-2% of the dry weight of the new shoots of tea plants (6). Theanine is the secondary metabolite conferring the umami taste of tea infusion and also balances the astringency and bitterness of tea infusion caused by catechins and caffeine (7). It has also many health-promoting functions, such as reducing stress and anxiety, improving mood and cognition, protecting the nervous system, etc (6, 8-13). Therefore, theanine content is highly correlated with green tea quality (14).

Theanine is synthesized from ethylamine (EA) and glutamate (Glu) by theanine synthetase (15, 16). Importantly, the large amount of theanine biosynthesis is determined by the high availability of EA in tea plants (17). Therefore, the evolution of EA biosynthesis in tea plants provided basis for theanine biosyntheis and the formation of tea quality. EA is synthesized from alanine decarboxylation by alanine decarboxylase (CsAlaDC) (18) (Figure 1A). Indeed, CsAlaDC expression level and catalytic activity largely determine the theanine accumulation level in tea plants (19). As a novel gene,

62 *CsAlaDC* had not been reported in other plant species before it was identified in tea
63 plants. Previous studies indicated that *AlaDC* originated from the serine decarboxylase
64 gene (*SerDC*) by gene duplication in tea plants (20). However, despite sharing highly
65 conserved amino acid sequences, CsAlaDC and CsSerDC specifically catalyze the
66 decarboxylation of alanine and serine, respectively (20) (Figure 1A, 1C). In addition,
67 CsAlaDC exhibited a much lower enzymatic activity compared with CsSerDC (20).
68 However, the structural basis and key amino acids underlying the evolution of the
69 substrate specificity and enzymatic activity of CsAlaDC are unknown.

70 SerDC belongs to the Group II pyridoxal-5-phosphate (PLP)-dependent
71 decarboxylase superfamily (21). These Group II amino acid decarboxylases produce
72 many bioactive secondary metabolites and signaling molecules (22-24). In plants,
73 SerDC catalyzes the biosynthesis of ethanolamine from serine, which was first
74 functionally characterized in *Arabidopsis thaliana* (25) (Figure 1A). Ethanolamine is
75 an important metabolite in the synthesis of phosphatidylethanolamine and
76 phosphatidylcholine, two main phospholipids involved in maintaining eukaryotic
77 membrane structures in eukaryotic cell membranes (26-28). Furthermore, the study has
78 shown that SerDC is essential in the embryogenesis of *Arabidopsis* (29). SerDC is of
79 vital importance for plant growth and development, but the mechanism of substrate
80 recognition and catalytic activity of SerDC also remains unclear.

81 In this work, we attempt to understand the mechanism of functional divergence of
82 plant AlaDC and SerDC by analyzing their structural characteristics. Here, we obtained
83 the X-ray crystal structure of CsAlaDC and AtSerDC. According to the crystal structure,

84 we found a distinctive zinc finger structure located at both CsAlaDC and AtSerDC,
85 which has not been identified in any other Group II PLP-dependent amino acid
86 decarboxylases that have been previously characterized. By comparing the substrate
87 binding pockets, we identified Phe^{106} of CsAlaDC and Tyr^{111} of AtSerDC as the crucial
88 sites for substrate specificity. By conducting mutation screening based on the protein
89 structures, we identified the amino acids repressing the catalytic activity and discovered
90 that $CsAlaDC^{L110F/P114A}$ exhibited a 2.3-fold increase in catalytic activity compared to
91 that of CsAlaDC and enhanced the engineering of theanine production *in vitro*.
92
93 **Results**
94 **Enzymatic properties of CsAlaDC, AtSerDC, and CsSerDC**
95 CsAlaDC originates from CsSerDC by gene duplication and neofunctionalization in tea
96 plants, but they catalyze different metabolic processes (Figure 1A). A phylogenetic tree
97 was constructed to further reveal the evolutionary relationship between CsAlaDC and
98 its homologs in *Algal*, *Pteridohyta*, *Bryophyta*, *Monocots* and *Dicots* (Figure 1B).
99 Phylogenetic analysis indicated that CsAlaDC is homologous with SerDCs in Dicots
100 plants. As expected, CsSerDC was closer to AtSerDC, which implies that they shared
101 similar functions. However, CsAlaDC is relatively distant from CsSerDC. Amino acid
102 sequence similarity analysis also showed that CsSerDC and AtSerDC had higher
103 smilarity than that between CsAlaDC and CsSerDC (Supplementary table 1). Next, we
104 performed a multiple sequence alignment of the amino acid sequences of the 6 SerDCs
105 from kiwifriut (*Actinidia chinensis*), grape (*Vitis vinifera*), coffee (*Coffea eugenioides*),

106 cocoa (*Theobroma cacao*), Arabidopsis and tea plants and CsAlaDC (Figure 1C). The
107 results showed that the amino acid sequences of CsAlaDC and SerDCs were highly
108 conserved, but CsAlaDC has amino acid mutations in highly conserved regions
109 compared with SerDCs.

110 Next, to verify the substrate specificity and enzyme activity, we conducted enzyme
111 activity detection and enzyme kinetics analysis for CsAlaDC, CsSerDC and AtSerDC.
112 The 5′ truncated *CsAlaDC* and *AtSerDC* were constructed into the pET22b and pET28a
113 expression vectors to generate recombinant plasmids pET22b-*CsAlaDC* and pET28a-
114 *AtSerDC*, correspondingly. Additionally, the full-length protein of CsSerDC was
115 inserted into the pET28a expression vector to generate recombinant plasmid pET28a-
116 *CsSerDC*. Subsequently, the recombinant proteins were expressed in *Escherichia coli*
117 and purified via nickel affinity chromatography. The purified proteins were examined
118 through SDS-PAGE analysis (Figure 2A). To investigate the substrate specificity of
119 CsAlaDC, AtSerDC, and CsSerDC, enzyme activity assays were conducted using Ala
120 and Ser as substrates, followed by product identification via UPLC analysis. The results
121 showed that CsAlaDC can effectively catalyzed the decarboxylation of alanine to
122 generate EA, whereas its catalytic efficacy towards serine was relatively inferior.
123 Conversely, AtSerDC and CsSerDC selectively catalyzed serine decarboxylation to
124 yield ethanolamine but did not exhibit activity towards alanine (Figure 2B). These
125 findings confirmed that CsAlaDC and SerDCs do not have promiscuous decarboxylase
126 activity on Ala and Ser.

127 The kinetic properties of CsAlaDC, AtSerDC, and CsSerDC were determined

through the use of corresponding substrates (Figure 2C), and the results are presented in Table 1. The kinetic parameter Km of CsAlaDC was determined to be 1.215 mM, which is similar to that of AtSerDC and CsSerDC at 1.522 mM and 2.364 mM, respectively. However, AtSerDC has a Vmax of 7.053 μmol/L/s, which is 4-fold that of CsAlaDC's Vmax of 1.709 μmol/L/s; while CsSerDC has a Vmax of 9.031 μmol/L/s, which is 5.3-fold that of CsAlaDC. These findings indicated that the catalytic efficiency of CsAlaDC is considerably lower than that of both CsSerDC and AtSerDC. The observed disparity in Vmax suggests that CsAlaDC and SerDCs may exhibit discrepancies in substrate-to-product conversion rates under saturated substrate conditions. It is plausible that SerDCs possess a higher turnover rate, facilitating the rapid conversion of substrate to product and subsequent release of the enzyme. Another possibility is that SerDCs demonstrate enhanced stability, thereby maintaining superior catalytic activity even at higher substrate concentrations, consequently leading to a higher Vmax value. Due to the similarity in catalytic activity between CsSerDC and AtSerDC, we chose the more representative AtSerDC for further analysis.

The overall structures of CsAlaDC and AtSerDC

To enhance our comprehension of CsAlaDC and AtSerDC, we conducted structural analyses of these two proteins. Through optimization of crystallization conditions, we successfully determined the crystal structures of CsAlaDC, CsAlaDC-EA, and AtSerDC at resolutions of 2.50 Å, 2.60 Å and 2.85 Å, respectively (Supplementary

table 2).

The overall structure of CsAlaDC and AtSerDC is homodimeric with two subunits exhibiting an asymmetrical arrangement (Figure 3A and 3D). The monomer of CsAlaDC or AtSerDC is divided into three distinct structural domains: an N-terminal domain (N-terminal -104 aa in CsAlaDC, N-terminal -109 aa in AtSerDC), a large domain (105-364 aa in CsAlaDC, 110-369 aa in AtSerDC), and a small C-terminal domain (365 aa-C-terminus in CsAlaDC, 370-C-terminus as in AtSerDC), colored light pink, khaki, and sky blue, respectively. Compared to the full-length protein, the N-terminal structures of CsAlaDC and AtSerDC were truncated by 60 and 65 amino acid residues, respectively. The N-terminal domain of the truncated protein contains a long α-helix, which is connected to the large domain through a long loop. The large domain contains a seven-stranded mixed β-sheet surrounded by eight α-helices, while the C-terminal domain is composed of a three-stranded antiparallel β-sheet and three α-helices (Supplementary figure 1). The catalytic site of the enzyme is positioned within a superficial crevice at the junction of two subunits forming a dimeric arrangement. The amino acid residues derived from both subunits participate in the binding of the PLP, effectively anchoring it to the active site. In the catalytic site, one monomer accommodates PLP, while the other monomer also contributes to PLP binding and enzymatic function (Figure 3A and 3D).

Notably, our investigation has revealed the presence of a distinctive zinc finger structure (as depicted in Figure 3A and 3D) located at the C-terminus of CsAlaDC and AtSerDC. This structure is composed of a loop structure spanning 17 amino acid

171 residues, wherein coordination of Zn^{2+} is facilitated by three Cys residues and one His
172 residue. Importantly, this particular configuration is exclusive to the two proteins under
173 examination and has not been identified in any other Group II PLP-dependent amino
174 acid decarboxylases that have been previously characterized (30, 31).

175 The crystal structures of CsAlaDC-EA complex and AtSerDC were obtained and
176 further analyzed. In the former complex, PLP bound to Lys^{309} via a Schiff base linkage
177 (internal aldimine form), and the pyridine moiety of PLP is positioned between the
178 imidazole ring of His^{196} and the methyl group of Ala^{279} in a parallel orientation to the
179 imidazole ring. The carboxylic group of Asp^{277} stabilizes the N1 of PLP by a salt bridge
180 interaction, providing the latter with the strong electrophilicity necessary to stabilize
181 carbon ion intermediates during enzymatic catalysis. The O3 forms hydrogen bonds
182 with Thr^{247} and Lys^{309}. Additionally, His^{308}, Gly^{169}, Thr^{170}, Lys^{309}, and Ser^{347}*("*"
183 denotes the amino acids on adjacent subunits) establish a hydrogen bonding network
184 with the phosphate group of PLP, consequently fortifying its attachment to the protein.
185 (Figure 3C). Similarly, in the latter structure, the pyridine ring of PLP was sandwiched
186 between the imidazole ring of His^{201} and the methyl group of Ala^{284}. The N1 of PLP
187 formed a salt bridge with Asp^{282}, while the O3 formed hydrogen bonds with Thr^{252}. The
188 phosphate group of PLP established hydrogen bonding interactions with Lys^{314}, His^{313},
189 Gly^{174}, Thr^{175}, and Ser^{352}* (Figure 3E). The aforementioned amino acid residues are
190 observed across various Group II PLP-dependent amino acid decarboxylases and
191 exhibit considerable stability (see further discussion below), suggesting that they could

192 share common features in terms of catalytic mechanisms.

193

194 **Factors affecting CsAlaDC and AtSerDC activity**

195 The Group II PLP-dependent amino acid decarboxylases are dimeric enzymes with
196 each monomer containing an active site located within a shallow cavity (32). A flexible
197 loop of amino acids originating from one monomer extends into the active site of the
198 other monomer and plays a crucial role in catalysis. The catalytic loop in CsAlaDC,
199 consisting of amino acid residues 328-341, is well-structured and exhibits clear electron
200 density. However, the corresponding loop in AtSerDC is disordered (Figure 3F). The
201 aforementioned loop harbors a conserved Tyr residue that is believed to function as a
202 proton donor of the carbanion in the catalytic process (33). In particular, CsAlaDC
203 Tyr^{336} and AtSerDC Tyr^{341} correspond to that Tyr residue (Supplementary figure 2).
204 Upon superimposing the active site residues of CsAlaDC apo and CsAlaDC-EA
205 complex, it was observed that the hydroxyl group of Tyr^{336}* in the CsAlaDC-EA
206 complex exhibits a substantial 60-degree deviation along the Cα-Cβ bond (Figure 3G).
207 To assess the function of the Tyr, we substituted the corresponding Tyr residues in
208 CsAlaDC and AtSerDC with Phe. The resulting $CsAlaDC^{Y336F}$ and $AtSerDC^{Y341F}$
209 mutants were then exposed to L-alanine and L-serine, respectively. We measured the
210 production of EA or ethanolamine in the reaction mixtures. Our findings indicate that
211 these mutants catalyze abortive decarboxylation, as opposed to wild-type CsAlaDC and
212 AtSerDC, as evidenced by the absence of detectable EA and only a small amount of
213 ethanolamine observed in the reaction mixture (Figure 3H). This result suggested this

214 Tyr is required for the catalytic activity of CsAlaDC and AtSerDC.

215

216 **Identification of key amino acids for the substrate specificity**

217 Through the superposition of the amino acid residues present in the substrate binding
218 pocket of CsAlaDC and AtSerDC, it was observed that the residues were identical,
219 except for Phe at position 106 in CsAlaDC (Figure 4A). In AtSerDC, this position is
220 occupied by Tyr at 111, implying that this specific amino acid residue is related to
221 substrate specificity.

222 To obtain more insights into the role of specific amino acid residue in substrate
223 specificity, we utilized amino acid sequences of AtSerDC to identify all potential serine
224 decarboxylases in *Embryophyta* and constructed phylogenetic trees (Supplementary
225 figure 3). We further identified conserved motifs in these SerDC homologs in
226 *Embryophyta* (Figure 4B). Importantly, the Phe^{106} of CsAlaDC or Tyr^{111} of AtSerDC
227 locates in a conserved motif (Figure 4B). In this conserved motif, the first two amino
228 acids Y and P are 100% conserved, but the third amino acid is variable and can be Y, T,
229 F, V, A, I, or other amino acids (Figure 4B and C); interestingly, the Phe^{106} of CsAlaDC
230 and Tyr^{111} of AtSerDC locates at this variable amino acid position. For these first three
231 amino acids, the YPY was identified in 83.7% of the SerDC homologs, while the YPF
232 motif was found in 2.3% of these SerDC homologs (Figure 4C). These analyses
233 provided more insights into the role of Phe^{106} of CsAlaDC and Tyr^{111} of AtSerDC in the
234 substrate specificity.

235 To verify the role of Phe^{106} of CsAlaDC or Tyr^{111} of AtSerDC in substrate specificity,

236 we mutated Phe^{106} of CsAlaDC into Tyr (CsAlaDC^{F106Y}) and Tyr^{111} of AtSerDC into
237 Phe (AtSerDC^{Y111F}) and tested enzymatic activity *in vitro*. The results showed that
238 CsAlaDC^{F106Y} totally lost the alanine decarboxylase activity, and AtSerDC^{Y111F} gained
239 alanine decarboxylase activity (Figure 4E). We also performed other mutations of Tyr^{111}
240 of AtSerDC, including AtSerDC^{Y111A}, AtSerDC^{Y111I}, AtSerDC^{Y111L}, AtSerDC^{Y111V} and
241 AtSerDC^{Y111W}. Within these mutations, only AtSerDC^{Y111I} exhibited a low level of
242 alanine decarboxylase activity (Figure 4E). These results verified that the Phe^{106} of
243 CsAlaDC is required for the alanine decarboxylase activity from serine decarboxylase
244 activity.

245 On the other side, both CsAlaDC and CsAlaDC^{F106Y} exhibit a very low level of
246 serine decarboxylase activity (Figure 4F). Moreover, compared with AtSerDC, the
247 serine decarboxylase activity of AtSerDC^{Y111F} was about 30% of AtSerDC;
248 AtSerDC^{Y111I} retained lower than 5% of serine decarboxylase activity of AtSerDC;
249 while other mutations, including AtSerDC^{Y111A}, AtSerDC^{Y111L}, AtSerDC^{Y111V} and
250 AtSerDC^{Y111W} abolished the serine decarboxylase activity (Figure 4F). These results
251 suggested the Tyr^{111} of AtSerDC is also important for the substrate specificity of
252 AtSerDC.

253 To further verify that Phe^{106} of CsAlaDC and Tyr111 of AtSerDC were key amino
254 acid residues determining its substrate recognition *in planta*, *Nicotiana benthamiana*
255 transient expression system was carried out. To this end, *A. tumefaciens* strain GV3101
256 (pSoup-p19), carrying recombinant plasmid, was infiltrated into leaves of 5-week-old
257 *N. benthamiana* plants, and the pCAMBIA1305 empty vector was used as the control

258 (EV). Relative mRNA levels were detected (Supplementary figure 4), indicating that
259 they had been successfully overexpressed in tobacco. Here, we found that a high level
260 of EA was produced in the CsAlaDC-expressing tobacco leaves; while no EA product
261 was detected in tobacco leaves infiltrated with the mutant CsAlaDC^{F106Y}. In addition,
262 we did not detect EA products in the AtSerDC-expressing tobacco leaves, while a high
263 level of EA was detected in tobacco leaves infiltrated with mutant AtSerDC^{Y111F}. As
264 anticipated, EA was not detected in tobacco leaves infiltrated with EV (Figure 4G and
265 H). These results further verified the critical role of Phe^{106} in the substrate specificity
266 of CsAlaDC.
267

268 **Key amino acids for the evolution of CsAlaDC enzymatic activity**

269 CsAlaDC and AtSerDC have a high sequence similarity of 74.5% and a nearly identical
270 structure with an RMSD (root mean square deviation) of only 0.77Å for monomer
271 structures. However, the two enzymes catalyze different amino acid decarboxylation
272 reactions, and AtSerDC exhibits significantly higher activity than CsAlaDC (Figure 2B
273 and C). To elucidate this observation, we proposed a prediction test: EA, generated via
274 Ala decarboxylation by CsAlaDC, can be toxic and harmful to plants if accumulated
275 excessively. Thus, during the evolution of plant serine decarboxylase into alanine
276 decarboxylase, the enzyme has evolved not just to alter the substrate preference but also
277 to reduce catalytic activity to control EA production within a suitable range. Based on
278 this hypothesis, we suggest that mutating specific amino acids in CsAlaDC to those
279 corresponding amino acids in SerDCs could enhance its activity, and the results could

280 provide insights into the evolution of CsAlaDC enzymatic activity.

281 Dimerization is essential to AlaDC/SerDC activities because the active site is
282 composed of residues from two monomers. To identify the amino acids repressing the
283 enzymatic activity of CsAlaDC during evolution from SerDC, we analyzed the crystal
284 structures and the amino acids at the dimer interface between CsAlaDC and AtSerDC.
285 This analysis revealed that the amino acid residues at positions 66, 97, 110, 114, 116,
286 117, 122, 315 and 345 are different in CsAlaDC and SerDCs (Figure 1C). Therefore,
287 we mutated these amino acids of CsAlaDC into those in the corresponding positions of
288 AtSerDC and CsSerDC, and performed enzyme activity assays (Figure 5A). The results
289 demonstrated that CsAlaDC^{L110F} and CsAlaDC^{P114A} exhibited significantly enhanced
290 enzyme activity compared to the wild-type CsAlaDC, with a 2.1-fold and 1.59-fold
291 increase, respectively. Furthermore, the catalytic activity of the CsAlaDC$^{L110F/P114A}$
292 double mutant exhibits a remarkable 2.3-fold increase compared to that of the wild-
293 type protein (Figure 5B). These findings suggested a critical role of Leu^{110} and Pro^{114}
294 of CsAlaDC in the evolution of enzymatic activity and provided a basis to improve
295 CsAlaDC activity. It is possible that these amino acid residues could potentially
296 augment the hydrophobic nature of the protein dimer interface.

297

298 ***In Vitro* synthesis of theanine**

299 The biosynthetic pathway of theanine in tea plants comprises two sequential enzymatic
300 steps: alanine decarboxylase mediates alanine decarboxylation to yield EA, which is
301 subsequently utilized by theanine synthetase to effectuate the condensation reaction

302 with glutamate to synthesize theanine. By conducting mutation screening, we
303 discovered a CsAlaDC mutant protein (L110F/P114A) that exhibited a 2.3-fold higher
304 catalytic activity compared to the wild-type protein. Subsequently, we employed an *in*
305 *vitro* theanine synthesis system utilizing CsAlaDC and either glutamine synthetase
306 (PtGS [P*seudomonas syringae* pv. syringae]) or gamma-glutamate methylamine ligase
307 (GMAS [*Methylovorus mays*]) which have the activity to synthesize theanine from EA
308 and Glu (34, 35).

309 The results illustrated the successful synthesis of theanine using CsAlaDC in
310 conjunction with two theanine synthetases, employing Ala and glutamate as substrates
311 (Figure 5C). The theanine content generated by the combination of $CsAlaDC^{L110F}$ and
312 GMAS, as well as $CsAlaDC^{L110F/P114A}$ and GMAS, was 4.57-fold and 6.72-fold higher
313 than the content produced in the combination of wild-type CsAlaDC and GMAS,
314 respectively. Similarly, when combined with the PsGS, comparable outcomes are
315 observed as well. The theanine content resulting from the combination of $CsAlaDC^{L110F}$
316 and PsGS, as well as $CsAlaDC^{L110F/P114A}$ and PsGS, exhibit enhancements of 1.62-fold
317 and 4.33-fold compared to the wild-type protein combination, respectively (Figure 5C).
318 Hence, the utilization of $CsAlaDC^{L110F/P114A}$ could effectively enhance the theanine
319 production yield and thus, holds potential for large-scale engineering production of
320 theanine.

321

322 **Discussion**

323 **Comparison of CsAlaDC and AtSerDC with other decarboxylases**

The Dali search (36) revealed that AtSerDC and CsAlaDC exhibit structural similarity to several other decarboxylases, including 7CIG (MetDC [*Streptomyces sp*. 590]), 7ERV (HisDC1 [*Photobacterium phosphoreum*]), 6KHO (TrpDC [*Oryza sativa Japonica* Group]), 4E1O (HisDC2 [*Homo sapiens*]), 6JY1 (AspDC [*Methanocaldococcus jannaschii*]), and 5GP4 (GluDC [*Levilactobacillus brevis*]). The monomers of these amino acid decarboxylases all consist of three characteristic domains (Figure 3 and Supplementary figure 6). The C-terminal domain, also known as the small domain, is composed of three antiparallel β-sheets and three α-helices, facing toward the opposite monomers. The large domain contains seven stranded β-sheets surrounded by eight α-helices, exhibiting characteristics typical of Type I enzymes. This domain includes a conserved PLP-binding active center and amino acid residues that are conserved across species. The N-terminal domain consists of elongated α-helices and is connected to the large domain via a loop. The helix of one subunit is antiparallel to the corresponding helix in the neighboring subunit, forming a clamp. Therefore, the N-terminal domain may not be an independent folding unit and is likely only stable in dimers.

The monomeric structure of CsAlaDC and AtSerDC exhibits numerous structural features common to other Group II PLP-dependent amino acid decarboxylases, and the amino acid residues that bind to PLP cofactors are conserved across multiple enzymes (Supplementary figure 5 and 6). Out of the eight proteins analyzed, a total of thirteen amino acid residues were found to be conserved across all sequences (Glu^{143}, Glu^{171}, Lys^{201}, Gly^{245}, Thr^{247}, Asp^{253}, His^{275}, Asp^{277}, Ala^{279}, Pro^{286}, Ser^{302}, Lys^{309}, and Tyr^{336} in

346 CsAlaDC). Some of them are situated within the active center and play a role in
347 stabilizing PLP or facilitating catalytic reactions. Conversely, other residues reside
348 outside the active center and their function remains unclear. (Supplementary figure 5).
349 PLP is bound to conserved lysine residues in the active center through the Schiff base.
350 The carboxylic group of conserved Asp residues stabilizes protonated pyridine nitrogen
351 of PLP by electrostatic action, providing the latter with strong electrophilicity to
352 stabilize carbanion intermediates during enzymatic catalysis. Another conserved His
353 residue is situated laterally to the PLP, while on the opposite side, there is a conserved
354 Ala residue. The oxygen atom at position 3 of PLP is stabilized by hydrogen bonding
355 with the Thr residue. The phosphate moiety of PLP is additionally secured to the protein
356 through an elongated system of hydrogen bonding. The α5 helix located within the large
357 domain exhibits evolutionary conservation in Group II enzymes, facilitating interaction
358 with the PLP phosphate moiety and conferring appropriate stabilization thereof.

359 The superimposition of the crystal structures of CsAlaDC and AtSerDC with those
360 of related enzymes suggests that residue Phe106 in CsAlaDC (corresponding to Tyr in
361 AtSerDC and Glu in MetDC) may play a role in determining substrate specificity. This
362 hypothesis was tested via mutagenesis experiments, which revealed that substitution of
363 Phe^{106} for Tyr rendered CsAlaDC inactive, while substitution of Tyr^{111} for Phe in
364 AtSerDC enabled alanine decarboxylase activity. Upon contemplation of these
365 experimental outcomes and informed by the elucidated crystal structures of both
366 enzymes, we speculate the hydrophilic nature of the Lys residue in AtSerDC
367 predisposes the active site to preferentially accommodate the hydrophilic amino acid

368 Ser as its substrate. In contrast, the analogous position in CsAlaDC is occupied by Phe,
369 an amino acid devoid of the hydroxyl moiety present in Lys, which augments the
370 hydrophobic character of the substrate-binding site. This structural nuance portends a
371 predisposition for CsAlaDC to select the comparatively hydrophobic amino acid
372 alanine as its suitable substrate. Likewise, the substitution of Glu^{64} for Ala in MetDC
373 reduced enzyme activity by approximately 50-fold compared to the wild-type (37),
374 bolstering the conclusion that the amino acid residue at this site influences the substrate
375 specificity of the enzyme.

376 Group II amino acid decarboxylase is characterized by the existence of highly
377 flexible catalytic rings, which are of great significance for the catalytic mechanism of
378 decarboxylase (33). The catalytic rings are located at the dimer interface and extend to
379 the active sites of other monomers in a closed conformation. In the structure of
380 CsAlaDC, the catalytic ring is orderly and allocated, while in the structure of AtSerDC,
381 it is disordered and lacks electron density (Figure 3F). Prior research has established
382 that the conserved amino acid residue Tyr within the ring plays a crucial role in catalysis
383 by donating protons to carbanions of quinone intermediates that arise following
384 decarboxylation (38, 39). Our experiments demonstrate that the substitution of the
385 corresponding Tyr with Phe in the loop renders the protein inactive. Furthermore,
386 alterations in the structure of CsAlaDC when combined with EA provide further
387 evidence supporting this conclusion. Specifically, the structure of CsAlaDC-EA
388 complex displayed a significant conformational change in Tyr^{336*} located in the
389 catalytic site (as depicted in Figure 3G). Comparing the structure of CsAlaDC apo, the

390 CsAlaDC-EA complex exhibited a notable 60-degree shift in the p-hydroxyl group of
391 Tyr^{336}* along the Cα-Cβ bond.

392 The monomeric configuration of CsAlaDC and AtSerDC is akin to that of other
393 Group II amino acid decarboxylases, except for a conspicuous dissimilarity. Unlike
394 other Group II amino acid decarboxylases, the C-terminal of CsAlaDC and AtSerDC
395 harbors an evident zinc finger structure. We propose that this structure could potentially
396 influence enzyme stability. To test this hypothesis, we truncated the zinc finger structure
397 from both proteins and expressed them. Our findings indicate that, following the
398 excision of the zinc finger structure, CsAlaDC became insoluble, while AtSerDC
399 displayed a similar trait to a certain extent.

400

401 **Evolution of AlaDC and SerDC**

402 The sequence identity between CsAlaDC and AtSerDC is 74.5%, indicating a
403 significant degree of homology. Moreover, the two proteins exhibit a high level of
404 monomer structural similarity. Notably, they differ in substrate specificity. Using the
405 crystal structure of CsAlaDC and AtSerDC as a basis, we identified pivotal amino acid
406 residues that govern the substrate specificity of serine or alanine decarboxylase. We
407 observed that sequences proximal to these sites exhibit a high degree of conservation
408 in both proteins and possess characteristic motifs (Figure 4B). Moreover, we analyzed
409 serine decarboxylase-like proteins in *Embryophyta* that are highly homologous to
410 CsAlaDC and constructed phylogenetic trees to gain insight into their evolutionary
411 relationships. Based on our experimental findings and evolutionary evidence, we have

412 identified a conserved YPX motif at the substrate binding pocket. For most plants, the
413 residue X in this motif is predominantly Tyr, which corresponds to the serine
414 decarboxylase protein. However, other residues such as Thr, Phe, Val, Ala, and Ile can
415 also occupy this position (Figure 4B and C). Interestingly, serine decarboxylase-like
416 proteins containing YPF motifs, which have the potential to function as alanine
417 decarboxylases, were found to be distributed throughout the phylogenetic tree,
418 including *Asteroideae*, *Ericales*, *Chenopodiaceae*, *Poaceae*, and *Ranunculales*
419 (Supplementary figure 3B). However, these proteins were absent in some more recent
420 species. This observation implies that the emergence of alanine decarboxylase in these
421 particular species could be attributed to convergent evolution.

422 Moreover, we have observed the enrichment of serine decarboxylase-like proteins
423 that possess a YPT motif within the *Fabales*. Prior research has demonstrated that
424 XP_004496485-1, which possesses a YPT motif, displays catalytic efficacy toward the
425 processes of decarboxylation and oxidative deamination of Phe, Met, Leu, and Trp (40).
426 Given that the YPT motif is highly conserved and widely distributed in *Fabales*, serine
427 decarboxylase-like proteins bearing the YPT motif may have developed a unique
428 substrate specificity in *Fabales*, beyond their conventional decarboxylation functions,
429 as exemplified by XP_004496485-1 protein mentioned above. We speculate that these
430 proteins may be capable of catalyzing other reactions, potentially involving non-protein

amino acids or other substances as substrates.

Applied to improve the synthesis of theanine

Theanine is an important indicator of green tea quality. Therefore, improving the synthesis of theanine in tea plants is the focus of research. In this study, through crystal structure analysis and mutation verification, we found that the catalytic activity of $CsAlaDC^{L110F/P114A}$ is 2.3 times higher than that of the wild-type protein, resulting in a more abundant synthesis of theanine *in vitro*. This gives us great inspiration to improve the synthesis of EA in tea plants by gene editing, thus increasing the content of theanine in tea plants (Figure 5).

Theanine is highly demanded, by the market, due to its health effects and medicinal value, and as a constituent in food, cosmetics and in other fields. To meet the market demand, a variety of methods have been used to acquire theanine, with the main methods including direct extraction, chemical synthesis, biotransformation (microbial fermentation) and plant cell culture. Based on this study, we can use mutation technology to modify engineering bacteria and improve the possibility of synthesis of theanine in bacteria, yeast, model plants, etc, promoting its use for industrial theanine production.

Conclusions

In conclusion, our structural and functional analyses have significantly advanced understanding of the substrate-specific activities of alanine and serine decarboxylases,

453 typified by CsAlaDC and AtSerDC. Critical amino acid residues responsible for
454 substrate selection were identified—Tyr111 in AtSerDC and Phe106 in CsAlaDC—
455 highlighting pivotal roles in enzyme specificity. The engineered CsAlaDC mutant
456 (L110F/P114A) not only displayed enhanced catalytic efficiency but also substantially
457 improved L-theanine yield in a synthetic biosynthesis setup with PsGS or GMAS. Our
458 research expanded the repertoire of potential alanine decarboxylases through the
459 discovery of 13 homologous enzyme candidates across embryophytic species and
460 uncovered a special motif present in serine protease-like proteins within *Fabale*,
461 suggesting a potential divergence in substrate specificity and catalytic functions. These
462 insights lay the groundwork for the development of industrial biocatalytic processes,
463 promising to elevate the production of L-theanine and supporting innovation within the
464 tea industry.
465

466 **Materials and Methods**

467 **Plants materials.**

468 Tobacco (*Nicotiana benthamiana*) plants were grown in a controlled chamber, under a
469 16-h light and 8-h dark photoperiod at 25 °C. Leaves of 5-week-old tobacco plants were
470 used for transient transformation, mediated by *Agrobacterium tumefaciens* strain
471 GV3101.
472

473 **Gene cloning and protein expression**

474 The coding sequences of AtSerDC and CsAlaDC, amino acid residues 66-482 and 61-

475 478, respectively, were amplified using PCR and then ligated into the *Nde* I and *Xho* I
476 restriction sites of the pET-28a and pET-22b vector, respectively, providing the
477 recombinant vector pET-28a-*AtSerDC* and pET-22b-*CsAlaDC*. The cDNAs encoding
478 CsSerDC were amplified using PCR and then ligated into the *Nde* I and *Xho* I restriction
479 sites of the pET-28a vector. Gene-specific primers were listed in Supplementary table
480 3. The recombinant plasmid was transformed into *E. coli* BL21 (DE3) competent cells.
481 Positive transformants were grown in a 5 mL LB medium containing 30 μg/mL
482 kanamycin or 50 μg/mL ampicillin at 37 ℃ overnight and then subcultured into an 800
483 mL LB medium containing the corresponding antibiotic. Protein expression was
484 induced by the addition of 0.2 mM isopropyl-β-d-thiogalactoside (IPTG) for 20 h at
485 16 ℃ when the optical density (OD) at 600 nm reached 0.6-0.8, harvested by
486 centrifugation at 4 °C and 4,000 rpm for 30 min.
487
488 **Protein production and crystallization**
489 The cell pellet was suspended in 30 mL of lysis buffer (20 mM HEPES, pH 7.5, 200
490 mM NaCl, 0.1 mM PLP), disrupted by High-Pressure Homogenizer, and then
491 centrifuged at 16,000 rpm for 30 min at 4 ℃ to remove the cell debris. The supernatants
492 were purified with a Ni-Agarose resin column followed by size-exclusion
493 chromatography. Before crystallization, purified proteins were concentrated at 10
494 mg/mL. Crystallization conditions were screened by the sitting-drop vapor diffusion
495 method using the reservoir solutions supplied in commercially available screening kits
496 (Crystal Screen, Crystal Screen 2, PEGRx 1, 2, and SaltRx 1, 2). A droplet made by

497 mixing 1.0 μL of purified AtSerDC or CsAlaDC (10 mg/mL) with an equal volume of
498 a reservoir solution was equilibrated against 100 μL of the reservoir solution at 16℃.
499 The crystal of AtSerDC was obtained using buffer pH 8.0 containing 20% (w/v)
500 PEG400 as a precipitate and 0.2 M $CaCl_2$. The crystal of the CsAlaDC-EA complex
501 was obtained at pH 7.5 containing 2.6 M sodium acetate. The crystal of CsAlaDC was
502 obtained at pH 6.0 containing 3.5 M sodium formate.
503
504 **Data collection and processing**
505 Crystals were grown by sitting-drop vapor diffusion method at 16 °C. The volume of
506 the reservoir solution was 100 μL and the drop volume was 2 μL, containing 1 μL of
507 protein sample and 1 μL of reservoir solution. The reservoir solution of AtSerDC
508 contained 0.1 M Tris-HCl (pH 8.0), 0.2 M $CaCl_2$, and 20% PEG 400. The reservoir
509 solution of CsAlaDC contained 0.1 M HEPES (pH 7.5), 2.6 M sodium acetate or 0.1 M
510 Bis-Tris (pH 6.0), and 3.5 M sodium formate. Crystals grew in 3-5 days using a protein
511 concentration of 10 mg/mL. Diffraction data were collected at Shanghai Synchrotron
512 Radiation Facility (China). The collected data sets were indexed, integrated, and scaled
513 using the HKL3000 software package. The structure of AtSerDC was solved by
514 molecular replacement using the structure of HisDC (PDB code: 7ERV
515 [*Photobacterium phosphoreum*]) as the model, and utilizing AtSerDC as a molecular
516 displacement model for both CsAlaDC and the CsAlaDC-EA complex. The AtSerDC,
517 CsAlaDC, and CsAlaDC-EA complex exhibit resolutions of 2.85 Å, 2.50 Å, and 2.60
518 Å, respectively. The statistics for data collection and processing are summarized in

519 Supplementary table 2.

520

521 **Enzyme activity assays**

522 Decarboxylase activity was measured by detecting products (EA or ethanolamine) in
523 Waters Acquit ultraperformance liquid chromatography (UPLC) system (20, 41). The
524 100 μL reaction mixture, containing 20 mM substrate (Ala or Ser), 100 mM potassium
525 phosphate, 0.1 mM PLP, and 0.025 mM purified enzyme, was prepared and incubated
526 at standard conditions (45 °C and pH 8.0 for CsAlaDC, 40 °C and pH 8.0 for AtSerDC
527 for 10 min). Then, the reaction was stopped with 20 μL of 10% trichloroacetic acid. The
528 product was derivatized with 6-aminoquinolyl-N-hydroxy-succinimidyl carbamate
529 (AQC) and subjected to analysis by UPLC. All enzymatic assays were performed in
530 triplicate.

531 The detection methodology for theanine production remains consistent with the
532 aforementioned approach. The 100 μL reaction mixture, containing 20 mM Ala, 45 mM
533 Glu, 50 mM HEPES (pH 7.5), 0.1 mM PLP, 30 mM $MgCl_2$, 10 mM ATP, 0.03 mM
534 PsGS/GMAS, and 0.025 mM CsAlaDC/CsAlaDC ^{L110F}/CsAlaDC $^{L110F/P114A}$, was
535 prepared and incubated at standard conditions for 1 h. Subsequently, the reaction was
536 terminated via immersion of the reaction vessel in a metal bath at 96 °C for 3 min (35).
537 Theanine was derivatized with AQC and subjected to analysis by UPLC. All enzymatic
538 assays were performed in triplicate.

539 **Site-directed mutagenesis**

540 Site-directed mutagenesis experiment was conducted using a PCR method from the

541 wild-type construct pET-28a-*AtSerDC* and pET-22b-*CsAlaDC*, respectively. *Dpn* I
542 endonucleases were used to digest the parental DNA template. The reaction mixture
543 was used to transform *E. coli* DH5α competent cells and the plasmids from positive
544 strains were extracted to *E. coli* BL21 (DE3) for protein expression, purification, and
545 analyzing the enzymatic activity.
546
547 ***In vivo* enzyme activity assay in *N. benthamiana***
548 The amplified PCR products were fused to the plant expression vector, pCAMBIA1305.
549 Linearization was conducted by restriction digest with *Spe* I and *Bam*H I. The
550 recombinant colonies were selected for PCR validation on the appropriate antibiotics
551 plate. After validation, the plasmids were electroporated into *Agrobacterium*
552 *tumefaciens* strain GV3101(pSoup-p19). Empty pCAMBIA1305 vector, with an intron
553 containing the GFP gene, was treated as the control.
554 *Agrobacterium* transient expression assays were performed on 5-week-old *N.*
555 *benthamiana* plants. *Agrobacterium tumefaciens* strain GV3101 (pSoup-p19), carrying
556 the above-described vectors, were cultured in Luria Bertani (LB) medium, containing
557 appropriate antibiotics, at 28 °C. When the absorbance of bacteria colonies reached
558 OD_{600} = 0.6-0.8, bacterial cells were collected and resuspended in MMA solution (10
559 mM $MgCl_2$, 10 mM 2-(N-morpholino) ethane sulfonic acid (MES), pH 5.6). After the
560 OD_{600} of the resuspended bacterial solution was adjusted to approx. 1.0, acetosyringone
561 (AS) was added with a final concentration of 200 μM, and this solution was then
562 incubated, at room temperature, for at least 3 h in darkness. Next, cell suspensions were

563 infiltrated into *N. benthamiana* leaves with a needle-free syringe. These *N.*
564 *benthamiana* leaves were then collected 3 days post infiltration, frozen in liquid
565 nitrogen and stored at -80 °C. Internal EA in *N. benthamiana* leaves was extracted as
566 previously described (22), and then the solvent was subjected to gas chromatography-
567 mass spectrometry GS-MS system.
568

569 **Transcript level analysis in *N. benthamiana***

570 Total RNA was isolated from samples using the RNAprep Pure Plant Kit (Tiangen,
571 Beijing, China), according to the manufacturer's protocol. The cDNAs were
572 synthesized using TransScript One-Step gDNA Removal and cDNA Synthesis
573 SuperMix Kit (TransGen Biotech, Beijing, China). The qRT-PCR assays were
574 performed, as previously described (42). Primers used for qRT-PCR assays were listed
575 in Supplementary table 4 and the qRT-PCR was run on a Bio-Rad CFX96TM RT PCR
576 detection system and CFX Manager Software. Each reaction reagent (20 μL) contained
577 0.4 μL forward and reverse primers (10 μM), 2 μL cDNA (200±5 ng/μL), 10 μL SYBR
578 Green Supermix (Vazyme, Nanjing, China) and 6.2 μL double-distilled water. Reaction
579 was performed by a two-step method: 95 °C for 5 min; 40 cycles of 95 °C for 10 s; and
580 60 °C for 30 s. The glyceraldehyde-3-phosphate dehydrogenase (GAPDH) gene was
581 used for internal normalization in each RT-PCR, and the $2^{-\Delta\Delta CT}$ method (43) was used
582 to calculate the relative gene expression. All samples were performed with three

583 replicates.

584

585 **Multiple sequence alignment**

586 MUSCLE was used to generate the protein multiple sequence alignment of amino acid
587 decarboxylases with default settings (44). ESPript 3.x was used to display the multiple
588 sequence alignment (45).

589

590 **Phylogenetic analysis**

591 The CsAlaDC was used as a query for searching its homologs in *Embryophyta* using
592 BLASTP (46) (version 2.13.0). To fetch homologs of CsAlaDC in distant species, we
593 performed a two-round blast. We first search for the best hit in the given order under
594 *Embryophyta*. Then we blast each species under a provided order using the order best
595 hit as a query and as many as 10 hits were kept. The sequences with e values <= 0.001
596 were removed. We further dropped sequences with lengths less than 200 or larger than
597 800 amino acids. Then multiple sequence alignment was performed via clustalo
598 (version 1.2.4) with default settings on these filtered sequences (47). The NJ algorithm
599 implemented in clustalw (version 2.1) was adopted to build the phylogenetic tree (48).
600 The R package ggtree (version 3.2.1) and universalmotif (version 1.12.4) were used for
601 tree and motif visualization (49).

602

603 **Acknowledgments**

604 We thank the team of beamline BL18U1 in the Shanghai Synchrotron Radiation Facility

for diffraction data collection.

Funding

This study is supported by grants from the Ministry of Science and Technology of China (2019YFA0904100 to W.G, 2022YFF1003103 to X.W) and the Natural Science Foundation of China (T2221005 to W.G, 32072624 to Z.Z).

Data availability

The structures of AtSerDC, CsAlaDC-EA complex and CsAlaDC have been deposited in the Protein Data Bank (PDB) under accession numbers 8JG7, 8JIK and 8JIJ respectively.

References

1. Drew, L. (2019) The growth of tea. *Nature* **566**, S2-S4.
2. Wheeler, D. S., Wheeler, W. J. (2004) The medicinal chemistry of tea. *Drug Dev. Res.* **61**, 45-65.
3. Xia, E. H. *et al*. (2017) The tea tree genome provides insights into tea flavor and independent evolution of caffeine biosynthesis. *Mol. Plant* **10**, 866-877.
4. Yang, C. S., Hong, J. G. (2013) Prevention of Chronic Diseases by Tea: Possible Mechanisms and Human Relevanc. *Annu. Rev. Nut.* **33**, 161-181.
5. Xia, E. *et al*. (2020) The reference genome of tea plant and resequencing of 81 diverse accessions provide insights into its genome evolution and adaptation. *Mol. Plant* **13**, 1013-1026.
6. Juneja, L. R., Chu, D. C., Okubo, T., Nagato, Y., Yokogoshi, H. (1999) L-theanine - a unique amino acid of green tea and its relaxation effect in humans. *Trends Food Sci.*

Technol. **10**, 425-425.

7. Lin, J. Z. *et al*. (2022) Effect of the presence of stem on quality of oolong tea. *Foods* **11**, 3439.
8. Haskell, C. F., Kennedy, D. O., Milne, A. L., Wesnes, K. A., Scholey, A. B. (2008) The effects of L-theanine, caffeine and their combination on cognition and mood. *Biol. Psychol.* **77**, 113-122.
9. Kakuda, T. *et al*. (2000) Protective effect of gamma-glutamylethylamide (theanine) on ischemic delayed neuronal death in gerbils. *Neuro. Sci. Lett.* **289**, 189-192.
10. Liu, Q., Duan, H., Luan, J., Yagasaki, K., Zhang, G. (2009) Effects of theanine on growth of human lung cancer and leukemia cells as well as migration and invasion of human lung cancer cells. *Cytotechnology* **59**, 211-217.
11. Lu, K. *et al*. (2004) The acute effects of L-theanine in comparison with alprazolam on anticipatory anxiety in humans. *Hum. Psychopharmacol.* **19**, 457-465.
12. Takagi, Y. *et al*. (2010) Combined administration of (L)-cystine and (L)-theanine enhances immune functions and protects against influenza virus infection in aged mice. *J. Vet. Med. Sci.* **72**, 157-165.
13. Zheng, G., Sayama, K., Okubo, T., Juneja, L. R., Oguni, I. (2004) Anti-obesity effects of three major components of green tea, catechins, caffeine and theanine, in mice. *In Vivo* **18**, 55-62.
14. Lin, S. *et al*. (2023) Theanine metabolism and transport in tea plants (*Camellia sinensis* L.): advances and perspectives. *Crit. Rev. Biotechnol*. **43**, 327-341.
15. Deng, W., Ogita, S., Ashihara, H. (2008) Biosynthesis of theanine (γ-ethylamino-l-glutamic acid) in seedlings of *Camellia sinensis*. *Phytochem. Lett.* **1**, 115-119.
16. Deng, W.-W., Ogita, S., Ashihara, H. (2009) Ethylamine content and theanine biosynthesis in different organs of camellia sinensis seedlings. *Z. Naturforsch. C* **64**, 906-906.
17. Cheng, S. *et al*. (2019) Differential accumulation of specialized metabolite L-theanine in green and albino-induced yellow tea (*Camellia sinensis*) leaves. *Food Chem.* 276, 93-100.
18. Takeo, T. (1974) L-alanine as a precursor of ethylamine in *Camellia sinensis*. *Phytochem.* **13**, 1401-1406.

19. Zhu, B. *et al*. (2021) CsAlaDC and CsTSI work coordinately to determine theanine biosynthesis in tea plants (*Camellia sinensis* L.) and confer high levels of theanine accumulation in a non-tea plant. *Plant Biotechnol. J.* **19**, 2395-2397.
20. Bai, P. *et al*. (2021) Biochemical characterization of specific Alanine Decarboxylase (ADC) and its ancestral enzyme Serine Decarboxylase (SDC) in tea plants (*Camellia sinensis*). *BMC Biotechnol.* **21**,17.
21. Han, S. W., Shin, J. S. (2022) Aromatic L-amino acid decarboxylases: mechanistic features and microbial applications. *Appl. Microbiol. Biotechnol.* **106**, 4445-4458.
22. Berger, M., Gray, J. A., Roth, B. L. (2009) The expanded biology of serotonin. *Annu. Rev. Med.* **60**, 355-366.
23. Khan, M. Z., Nawaz, W. (2016) The emerging roles of human trace amines and human trace amine-associated receptors (hTAARs) in central nervous system. *Biomed. Pharmacother*. **83**, 439-449.
24. Ng, J., Papandreou, A., Heales, S. J., Kurian, M. A. (2015) Monoamine neurotransmitter disorders--clinical advances and future perspectives. *Nat. Rev. Neurol.* **11**, 567-584.
25. Rontein, D. *et al*. (2001) Plants synthesize ethanolamine by direct decarboxylation of serine using a pyridoxal phosphate enzyme. *J. Biol. Chem.* **276**, 35523-35529.
26. Gibellini, F., Smith, T. K. (2010) The Kennedy pathway-De novo synthesis of phosphatidylethanolamine and phosphatidylcholine. *IUBMB Life* **62**, 414-428.
27. Mudd, S. H., Datko, A. H. (1989) Synthesis of ethanolamine and its regulation in *Lemna paucicostata*. *Plant Physiol.* **91**, 587-597.
28. Zinser, E. *et al*. (1991) Phospholipid synthesis and lipid composition of subcellular membranes in the unicellular eukaryote *Saccharomyces cerevisiae*. *J. Bacteriol.* **173**, 2026-2034.
29. Yunus, I. S., Liu, Y.-c., Nakamura, Y. (2016) The importance of SERINE DECARBOXYLASE1 (SDC1) and ethanolamine biosynthesis during embryogenesis of *Arabidopsis thaliana*. *Plant J.* **88**, 559-569.
30. Komori, H. et al. (2012) Structural Study Reveals That Ser-354 Determines Substrate Specificity on Human Histidine Decarboxylase* *J Biol Chem.* **287**, 29175-83.

31. Huang, J. et al. (2018) Lactobacillus brevis CGMCC 1306 glutamate decarboxylase: Crystal structure and functional analysis. *Biochem Biophys Res Co*. **503**, 1703-1709
32. Paiardini, A., Giardina, G., Rossignoli, G., Voltattorni, C. B., Bertoldi, M. (2017) New insights emerging from recent investigations on human group II pyridoxal 5'-phosphate decarboxylases. *Curr. Med. Chem.* **24**, 226-244.
33. Torrens-Spence, M. P. *et al*. (2020) Structural basis for divergent and convergent evolution of catalytic machineries in plant aromatic amino acid decarboxylase proteins. *Proc. Natl. Acad. Sci. U. S. A.* **117**, 10806-10817.
34. Hagihara, R., Ohno, S., Hayashi, M., Tabata, K., Endo, H. (2021) Production of L-theanine by *Escherichia coli* in the absence of supplemental ethylamine. *Appl. Environ. Microbiol.* **87**, e00031-21.
35. Yamamoto, S., Wakayama, M. & Tachiki, T. (2007) Characterization of theanine-forming enzyme from *Methylovorus mays* no. 9 in respect to utilization of theanine production. *Biosci. Biotechnol. Biochem.* **71**, 545-552.
36. Holm, L. (2022) Dali server: structural unification of protein families. *Nucleic. Acids Res.* **50**, W210-W215.
37. Okawa, A. *et al*. (2021) Structural basis for substrate specificity of L-methionine decarboxylase. *Protein Sci.* **30**, 663-677.
38. Fenalti, G. *et al*. (2007) GABA production by glutamic acid decarboxylase is regulated by a dynamic catalytic loop. *Nat. Struct. Mol. Biol.* **14**, 280-286.
39. Gayathri, S. C., Manoj, N. (2019) Structural insights into the mechanism of internal aldimine formation and catalytic loop dynamics in an archaeal Group II decarboxylase. *J. Struct. Biol.* **208**, 137-151.
40. Torrens-Spence, M. P., von Guggenberg, R., Lazear, M., Ding, H., Li, J. (2014) Diverse functional evolution of serine decarboxylases: identification of two novel acetaldehyde synthases that uses hydrophobic amino acids as substrates. *BMC Plant Biol.* **14**, 247.
41. Qu, L., Gu, S., Zhang, J., Zhao, C., Deng, X. (2021) Determination of 18 amino acids in three different kinds of milk powder by ultra performance liquid chromatography coupled with pre-column derivatization. *Chin. J. Chromatogr.* **39**, 472-477.

42. Madeira, F. *et al*. (2022) Search and sequence analysis tools services from EMBL-EBI in 2022. *Nucleic Acids Res.* **50**, W276-W279.
43. Dong C. *et al*. (2020) Theanine transporters identified in tea plants (*Camellia sinensis* L.). *Plant J.* **101**, 57-70.
44. Schmittgen T. D. *et al*. (2000) Quantitative reverse transcription-polymerase chain reaction to study mRNA decay: comparison of endpoint and real-time methods. *Anal. Biochem.* **285**, 194–204.
45. Robert X., Gouet P. (2014) Deciphering key features in protein structures with the new ENDscript server. *Nucleic Acids Res.* **42**, W320-W324.
46. Camacho, C. *et al*. (2009) BLAST+: architecture and applications. *BMC Bioinf.* **10**, 421.
47. Sievers, F., Higgins, D. G. (2018) Clustal Omega for making accurate alignments of many protein sequences. *Protein Sci.* **27**, 135-145.
48. Larkin, M. A. *et al*. (2007) Clustal W and clustal X version 2.0. *Bioinformatics.* **23**, 2947-2948.
49. Yu, G., Lam, T. T.-Y., Zhu, H., Guan, Y. (2018) Two methods for mapping and visualizing associated data on phylogeny using ggtree. *Mol. Biol. Evol.* **35**, 3041-3043.

Figures and table

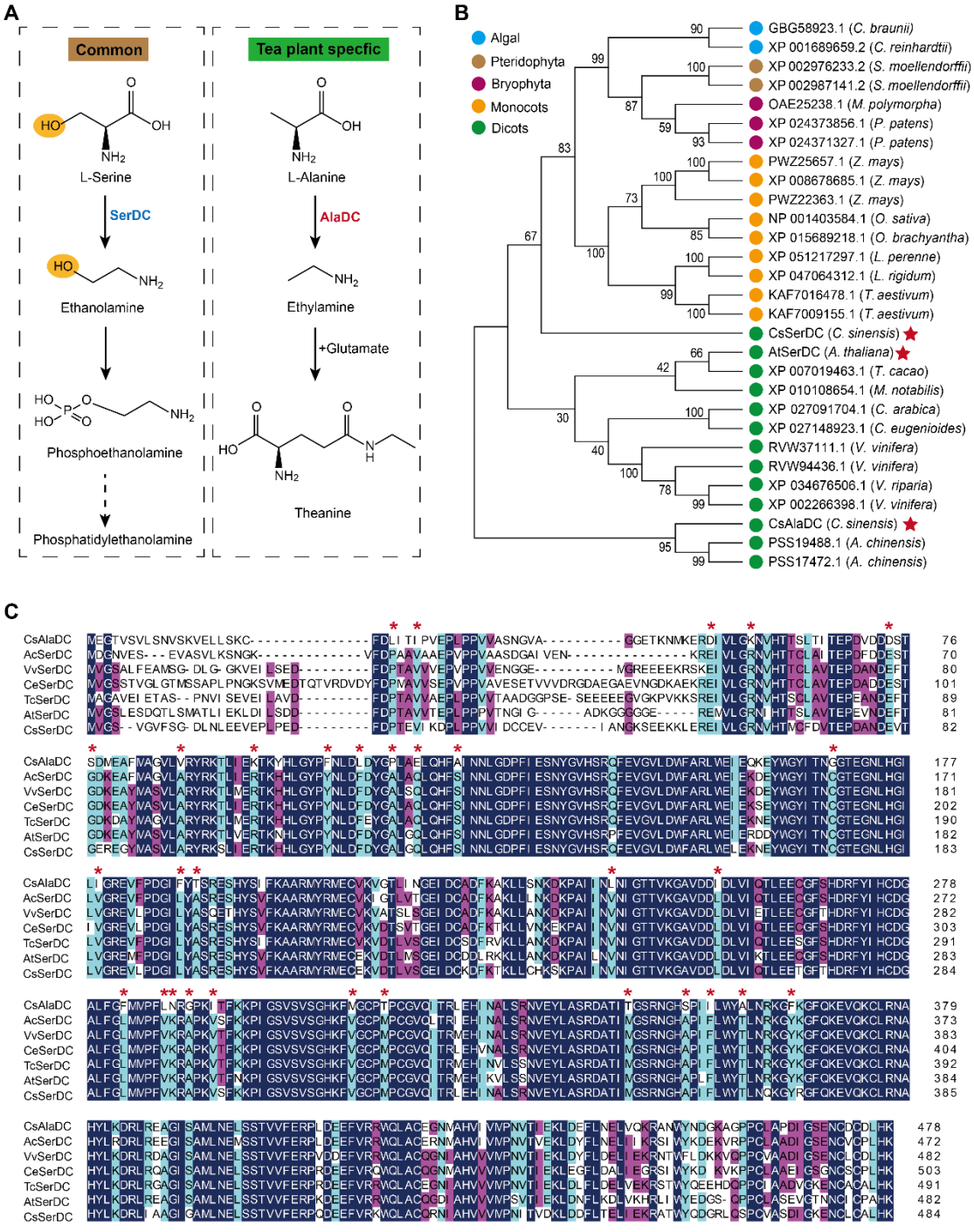

Figure 1. Metabolic pathways and phylogeny analysis of SerDC and AlaDC in plants. (**A**) The decarboxylation of serine and alanine in plants. SerDC, serine decarboxylase; AlaDC, alanine decarboxylase. (**B**) Phylogenetic analysis of the SerDC homologous proteins in Algal, Pteridohyta, Bryophyta, Dicots and Monocots. The

742 phylogenetic tree was performed using the neighbor-joining method in MAGA 7.0
743 software and bootstrap values based on 1000 replicates were displayed at branch points.
744 These proteins were represented by their GenBank accession number. (**C**) Multiple
745 alignment of the amino acid sequences of AlaDC and SerDCs. Primary (100%),
746 secondary (80%), and tertiary (60%) conserved percent of similar amino acid residues
747 were shaded in deep blue, light blue and cheer red, respectively. The multiple alignment
748 was constructed by MAGA 7.0 software by ClustalW method, and GeneDOC software
749 was used to visualize multiple sequence alignments. "*" indicated amino acid residues
750 mutated only in CsAlaDC.
751
752
753

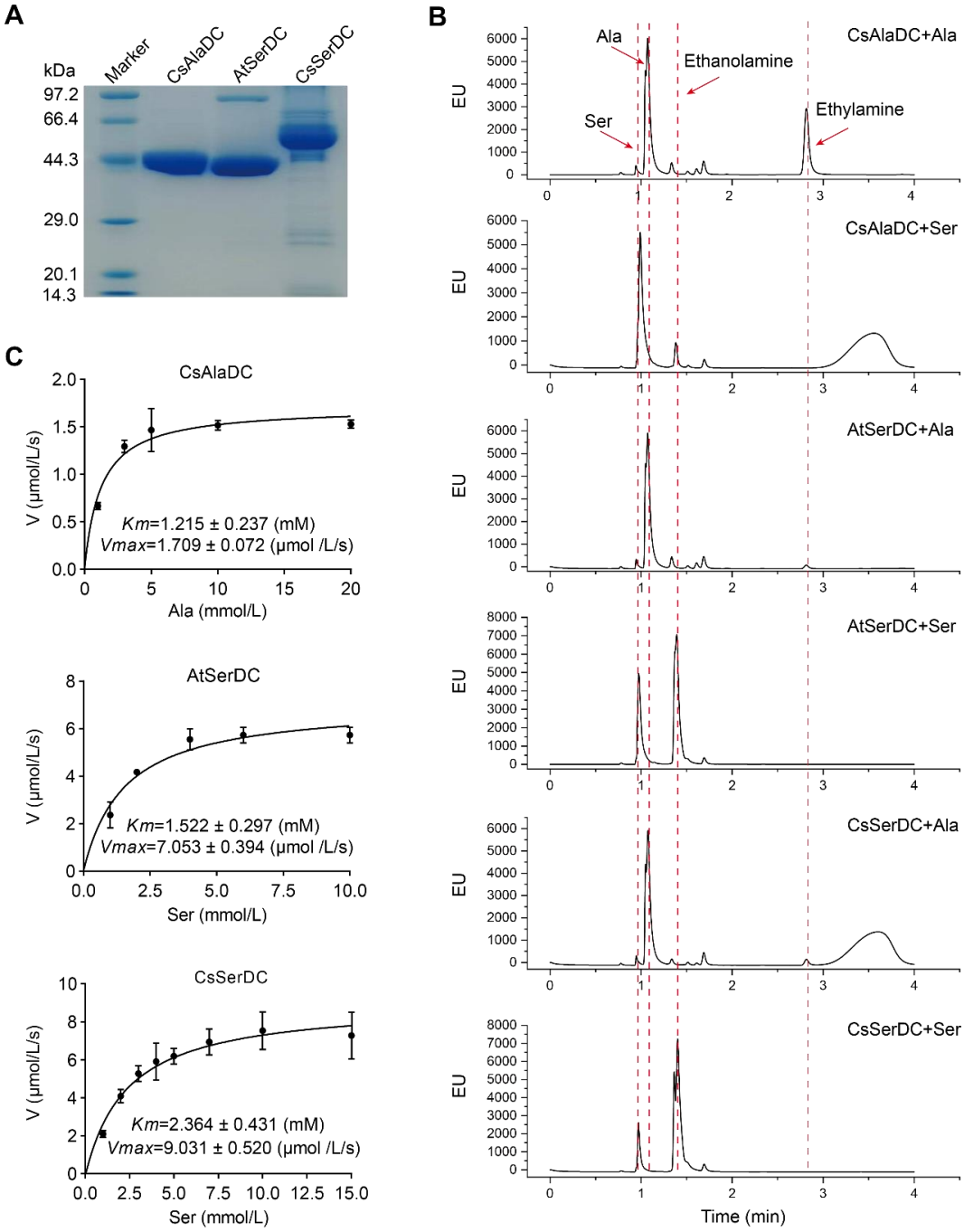

Figure 2. Purification and characterization of CsAlaDC, AtSerDC, and CsSerDC. (**A**) Identification of CsAlaDC, AtSerDC, and CsSerDC using SDS-PAGE. (**B**) Detection of enzyme activities of CsAlaDC, AtSerDC, and CsSerDC by UPLC. (**C**) Reaction rates of substrates with different concentrations catalyzed by CsAlaDC, AtSerDC, and CsSerDC.

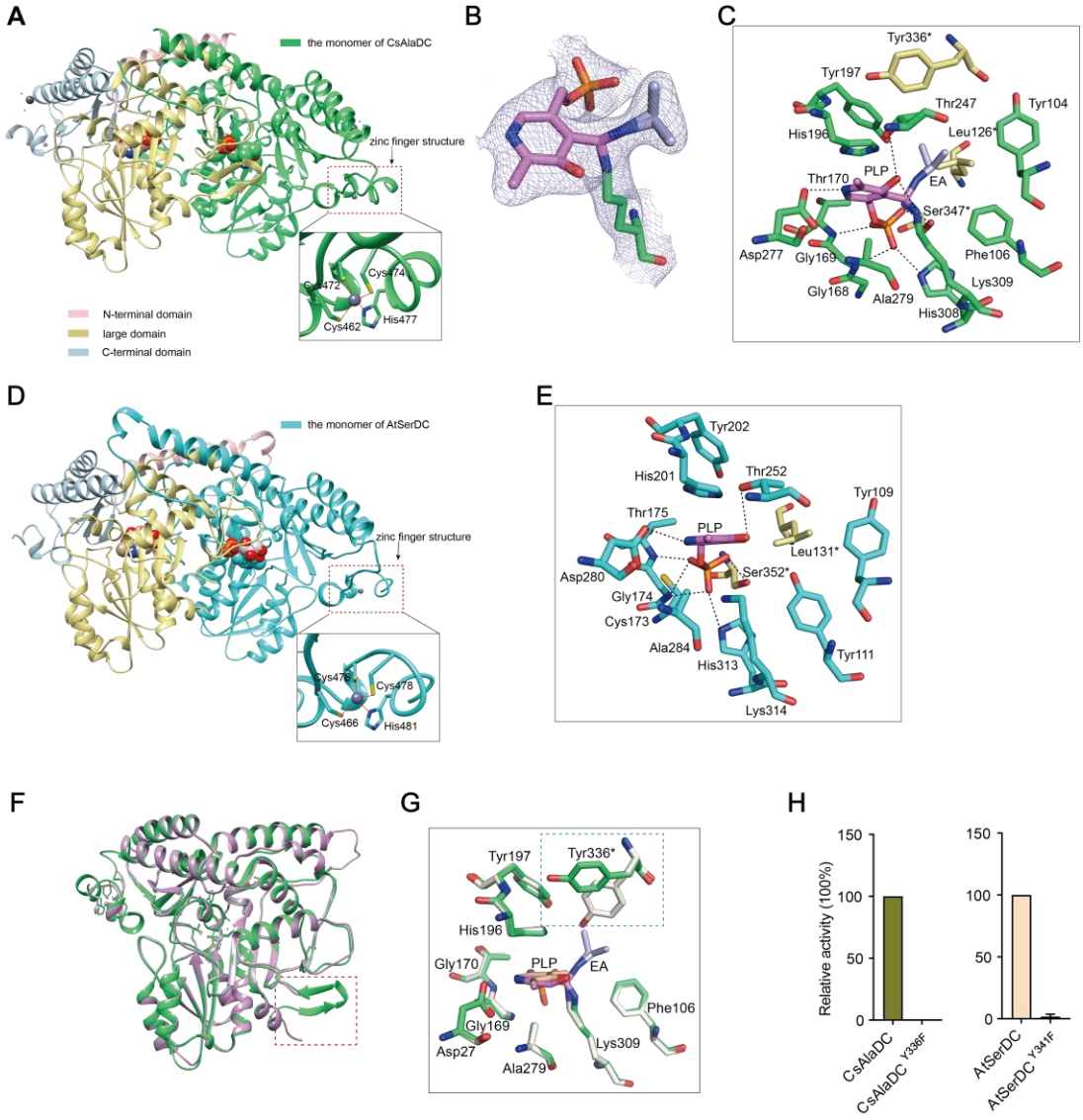

Figure 3. Crystal structures of CsAlaDC and AtSerDC. (**A**) Dimer structure of CsAlaDC. The color display of the N-terminal domain, large domain, and C-terminal domains of chain A is shown in light pink, khaki and sky blue, respectively. Chain B is shown in spring green. The PLP molecule is shown as a sphere model. The zinc finger structure at the C-terminus of CsAlaDC is indicated by the red box. The gray spheres represent zinc ions, while the red dotted line depicts the coordination bonds formed by zinc ions with cysteine and histidine. (**B**) The 2Fo-Fc electron density maps of K309-PLP-EA (contoured at 1σ level). The PLP is shown in violet, the K309 is shown in

770 spring green, and the EA is shown in lightblue. (**C**) Active center of the CsAlaDC-EA
771 complex, with hydrogen bonds denoted by black dotted lines. "*" denotes the amino
772 acids on adjacent subunits. (**D**) Dimer structure of AtSerDC. The color display of the
773 N-terminal domain, large domain, and C-terminal domains of chain A is shown in light
774 pink, khaki and sky blue, respectively. Chain B is shown in cyan. The PLP molecule is
775 shown as a sphere model. The zinc finger structure at the C-terminus of AtSerDC is
776 indicated by the red box. The gray spheres represent zinc ions, while the red dotted line
777 depicts the coordination bonds formed by zinc ions with cysteine and histidine. (**E**)
778 Active center of the AtSerDC, with hydrogen bonds denoted by black dotted lines. "*"
779 denotes the amino acids on adjacent subunits. (**F**) The monomers of CsAlaDC and
780 AtSerDC are superimposed. CsAlaDC is depicted in spring green, while AtSerDC is
781 shown in plum. The conserved amino acid catalytic ring is indicated by the red box. (**G**)
782 Amino acid residues of the active center in CsAlaDC apo and CsAlaDC-EA complex
783 are superimposed. CsAlaDC apo is shown in floral white, while CsAlaDC-EA complex
784 is shown in spring green. (**H**) The relative activity of wild-type CsAlaDC and its Y336F
785 mutant (left), as well as wild-type AtSerDC and its Y341F mutant (right) is shown.
786

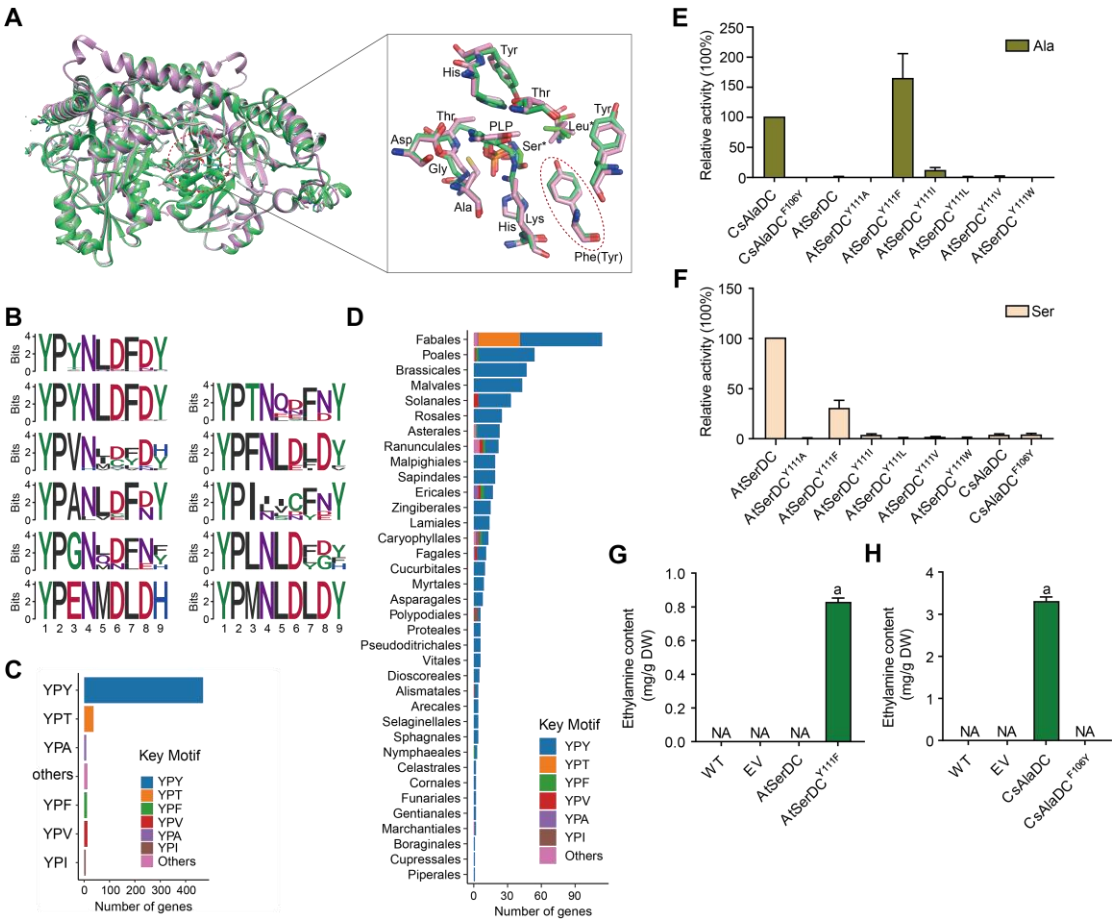

Figure 4. Key amino acid residues for substrate recognition. (**A**) Superposition of substrate binding pocket amino acid residues in CsAlaDC and AtSerDC. The amino acid residues of CsAlaDC are shown in spring green, the amino acid residues of AtSerDC are shown in plum, with the substrate specificity-related amino acid residue highlighted in a red ellipse. (**B**) Active-site-lining residues from *Embryophyta* AlaDC were identified. The height of the residue label displays the relative amino acid frequency. (**C**) Histogram showing the distribution of the number of key motifs. (**D**) Histogram showing the number of key motifs in different plant orders. (**E**) Relative enzyme activities of wild-type CsAlaDC and mutant protein CsAlaDC^{F106Y} against Ala substrate (columns 1 and 2), and enzyme activities of wild-type AtSerDC and various

798 AtSerDC mutant proteins against Ala substrate (columns 3-9) are presented. The
799 percentage graph shows the relative activity of each protein compared to wild-type
800 CsAlaDC activity (taken as a 100% benchmark). (**F**) Relative enzyme activities of wild-
801 type AtSerDC and AtSerDC mutant proteins (columns 1-7) against Ser substrates, and
802 enzyme activities of wild-type CsAlaDC and mutant protein CsAlaDC^{F106Y} against Ser
803 substrates(columns 8, 9) were measured. The percentage graph shows the relative
804 activity of each protein compared to the wild-type AtSerDC (taken as a 100%
805 benchmark). Three independent experiments were conducted. (**G**) The EA contents of
806 AtSerDC and its mutant AtSerDC^{Y111F} in *N. benthamiana*. (**H**) The EA contents of
807 CsAlaDC and its mutant CsAlaDC^{F106Y} in *N. benthamiana*. The significance of the
808 difference (P<0.05) was labeled with different letters according to Duncan's multiple
809 range test.

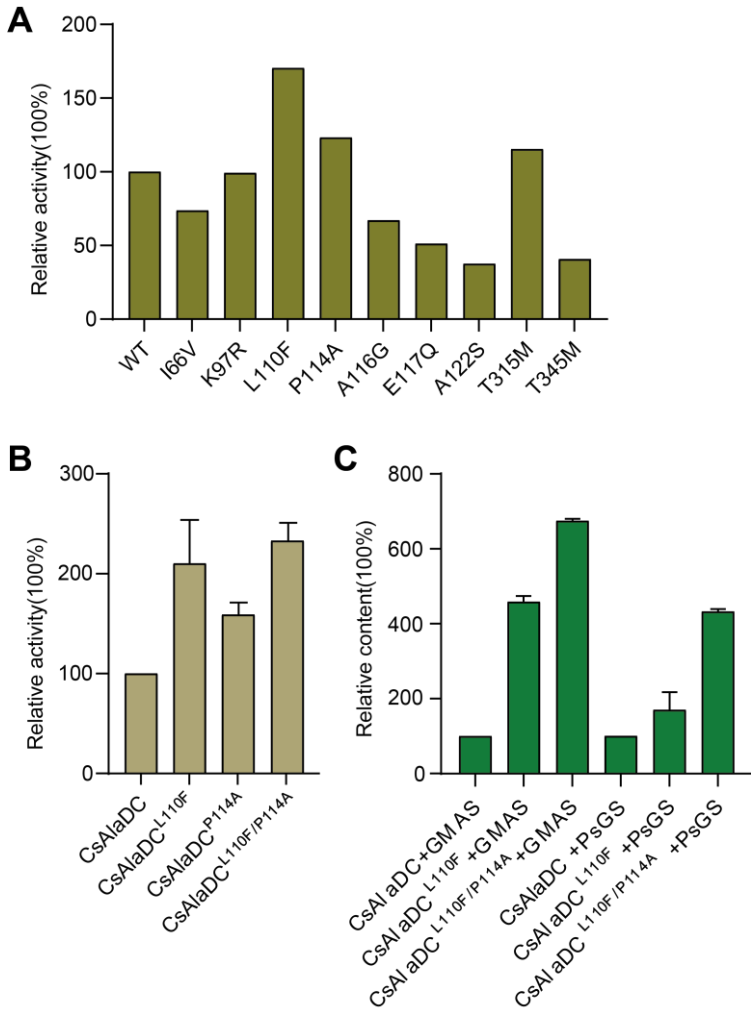

Figure 5. Mutations enhance CsAlaDC enzyme activity and theanine synthesis *in vitro*. (**A**) Relative enzyme activities of CsAlaDC mutant proteins against Ala substrate. (**B**) Relative enzyme activities of CsAlaDC^{L110F}, CsAlaDC^{P114A}, and CsAlaDC$^{L110F/P114A}$ against Ala substrate. (**C**) Histogram showing the relative content of theanine resulting from different combinations of alanine decarboxylase and theanine synthetase. Three independent experiments were conducted.

818 **Table 1.** Kinetic parameters of CsAlaDC, AtSerDC and CsSerDC

Enzyme	Substrate	*Km* (mM)	*Vmax* (μmol/L/s)
CsAlaDC	Alanine	1.215 ± 0.237	1.709 ± 0.072
AtSerDC	Serine	1.522 ± 0.297	7.053 ± 0.297
CsSerDC	Serine	2.364 ± 0.431	9.031 ±0.520

819

820

821

822 **Supplementary figures**

823

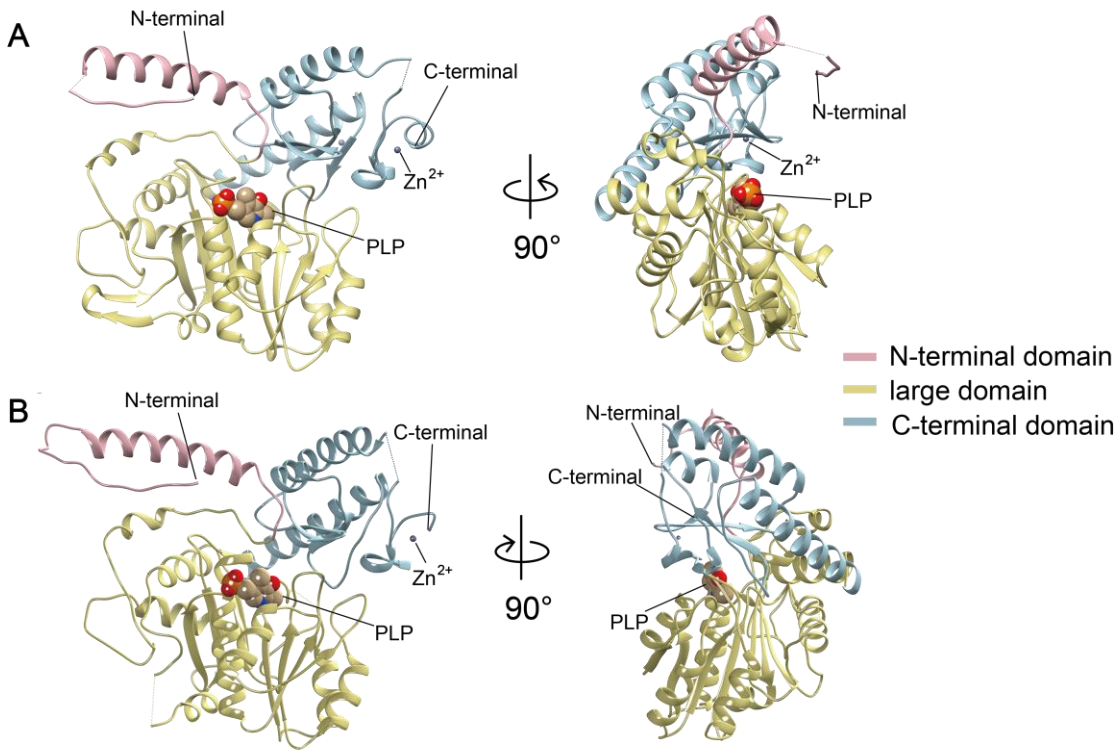

824

825 **Supplementary figure 1. Crystal structures of CsAlaDC and AtSerDC**. (**A**)
826 Monomer structure of CsAlaDC. (**B**) Monomer structure of AtSerDC. The color display
827 of the N-terminal domain, large domain, and C-terminal domains is shown in light pink,
828 khaki and sky blue, respectively. The PLP molecule is shown as a sphere model. The
829 gray spheres represent zinc ions.

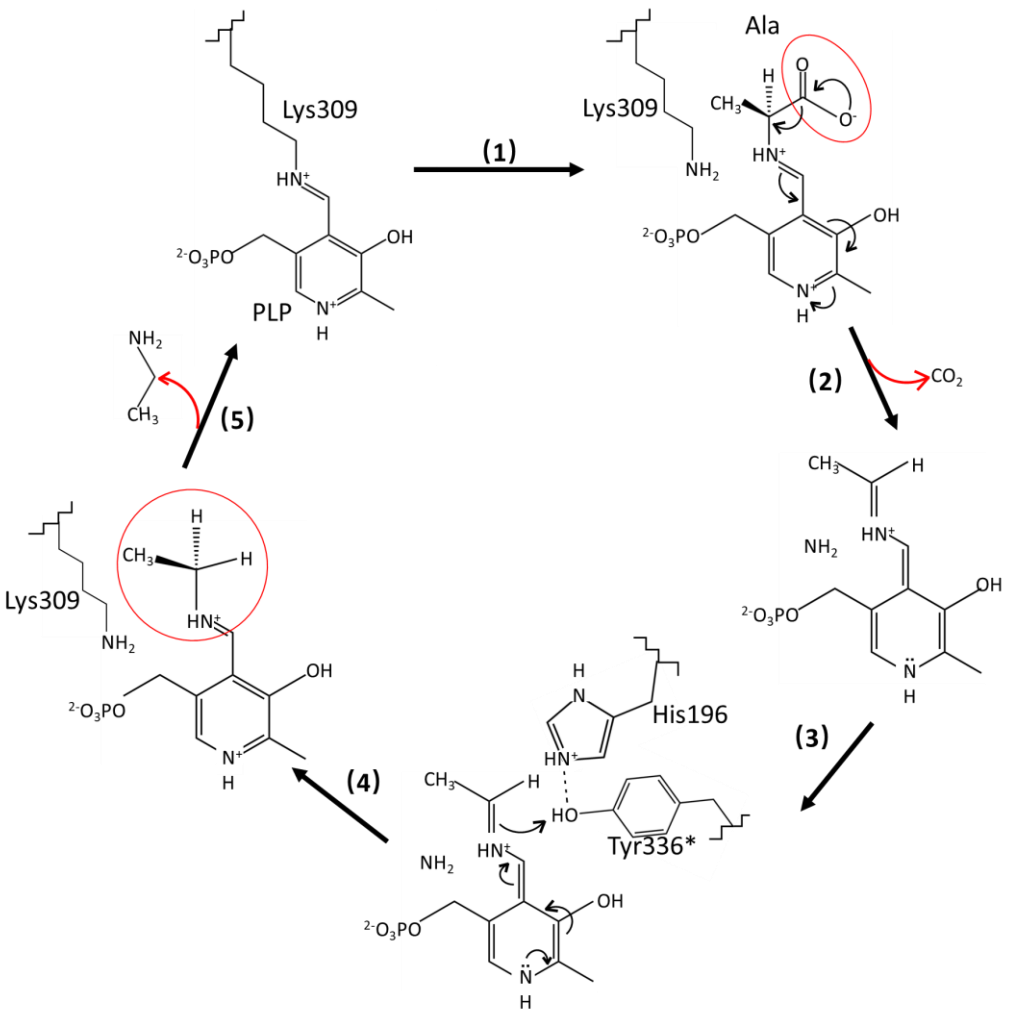

Supplementary figure 2. Catalytic mechanisms and conformational changes of CsAlaDC. After the transaldimation of the internal aldimine within CsAlaDC, resulting in the release of the active-site residue Lys309, the PLP amino acid external aldimine undergoes decarboxylation, leading to the removal of the α-carboxyl group as CO2. This process generates a quinonoid intermediate that is stabilized by the delocalization of paired electrons (1,2). The carbanion at Cα is subsequently protonated by the acidic p-hydroxyl group of Tyr336* located on the large loop, facilitated by its neighboring residue His196, which is situated on the small loop (3,4). Simultaneously, the internal aldimine LLP309 in CsAlaDC is restored, resulting in the release of the product (5).

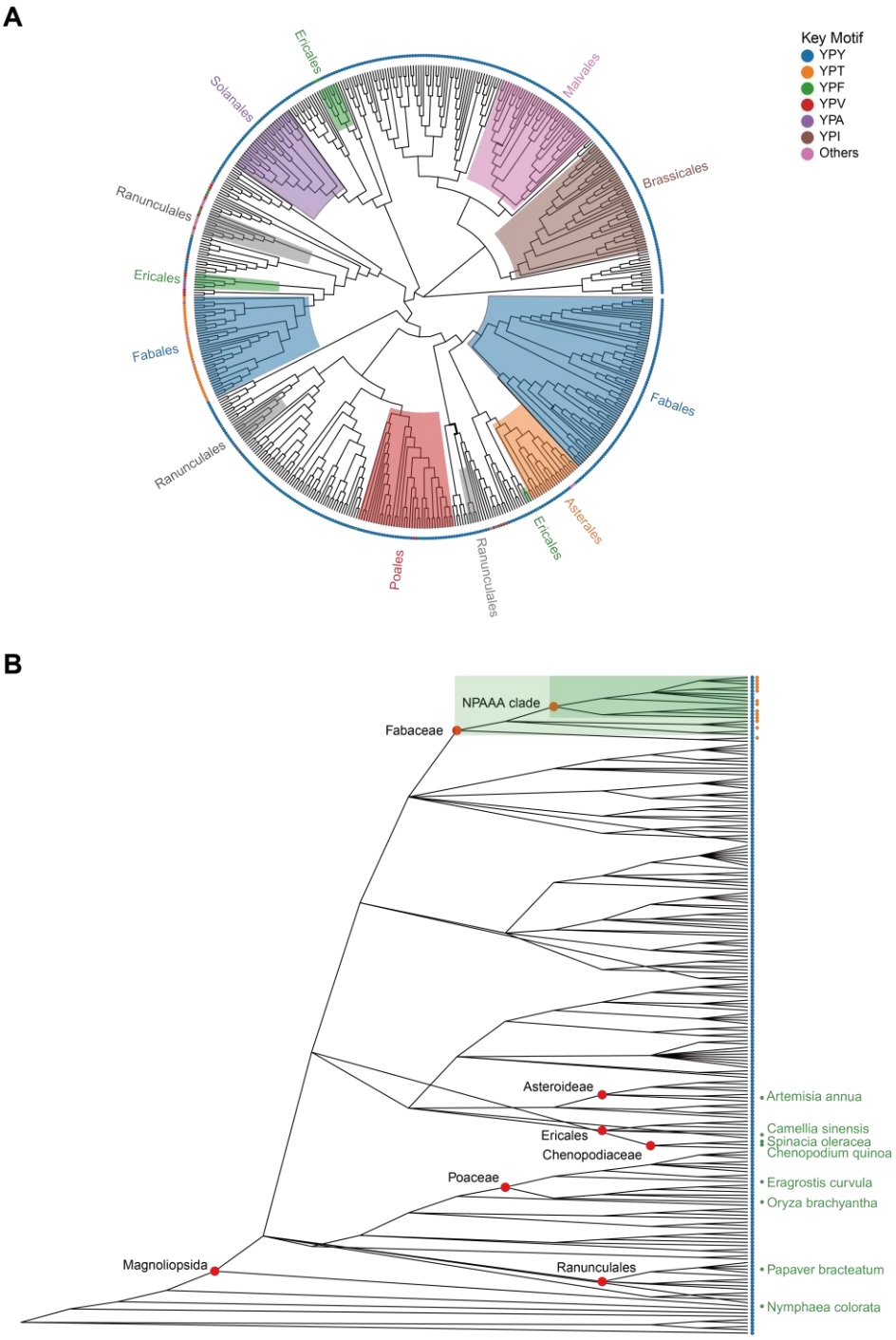

Supplementary figure 3. Evolutionary analysis of CsAlaDC in *Embryophyta*. (**A**) The presented diagram depicts an evolutionary tree of CsAlaDC, which is devoid of a root and solely portrays the topological structure of the tree without including distance information. The color of the inner ring corresponds to various orders, while the outer ring's leaf nodes are colored based on the motif types that the sequence exhibits. (**B**)

Diversity of serine decarboxylase-like proteins in *Embryophyta* (196 species). Colored scatter spots on the right side of leaf nodes correspond to the respective motifs shown in Figure A.

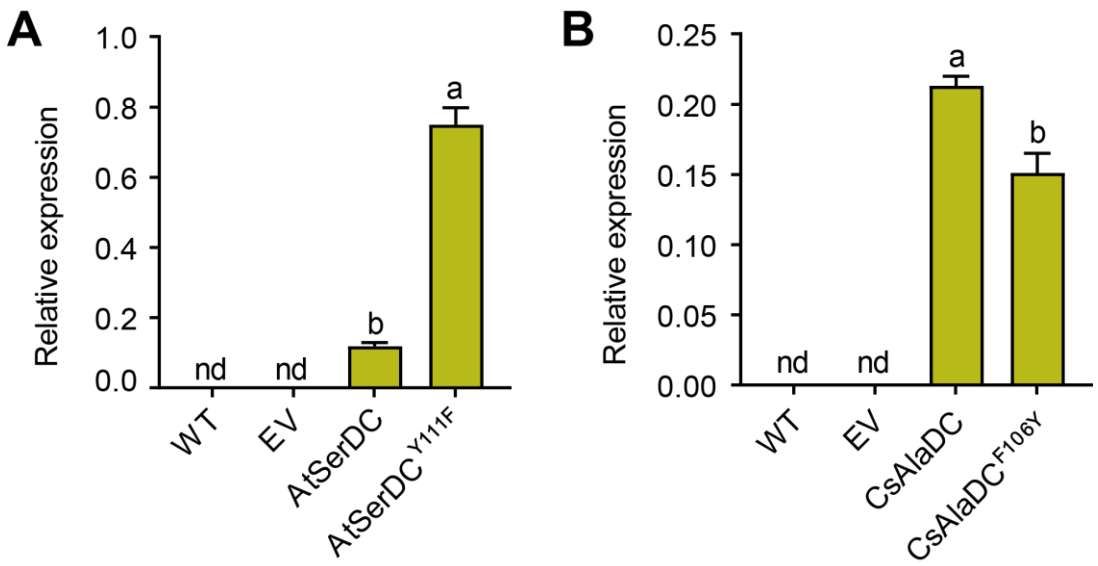

Supplementary figure 4. The relative mRNA levels of AtSerDC and its mutant Y111F (*A*), CsAlaDC and its mutant F106Y (*B*) in *N. benthamiana* leaves were measured by two primers. WT, wild type of *N. benthamiana*; EV, empty vector control; *NbGAPDH* was used as an internal control. Data represent mean ± SD (n=3). The significance of the difference (P<0.05) was labeled with different letters according to Duncan's multiple range test.

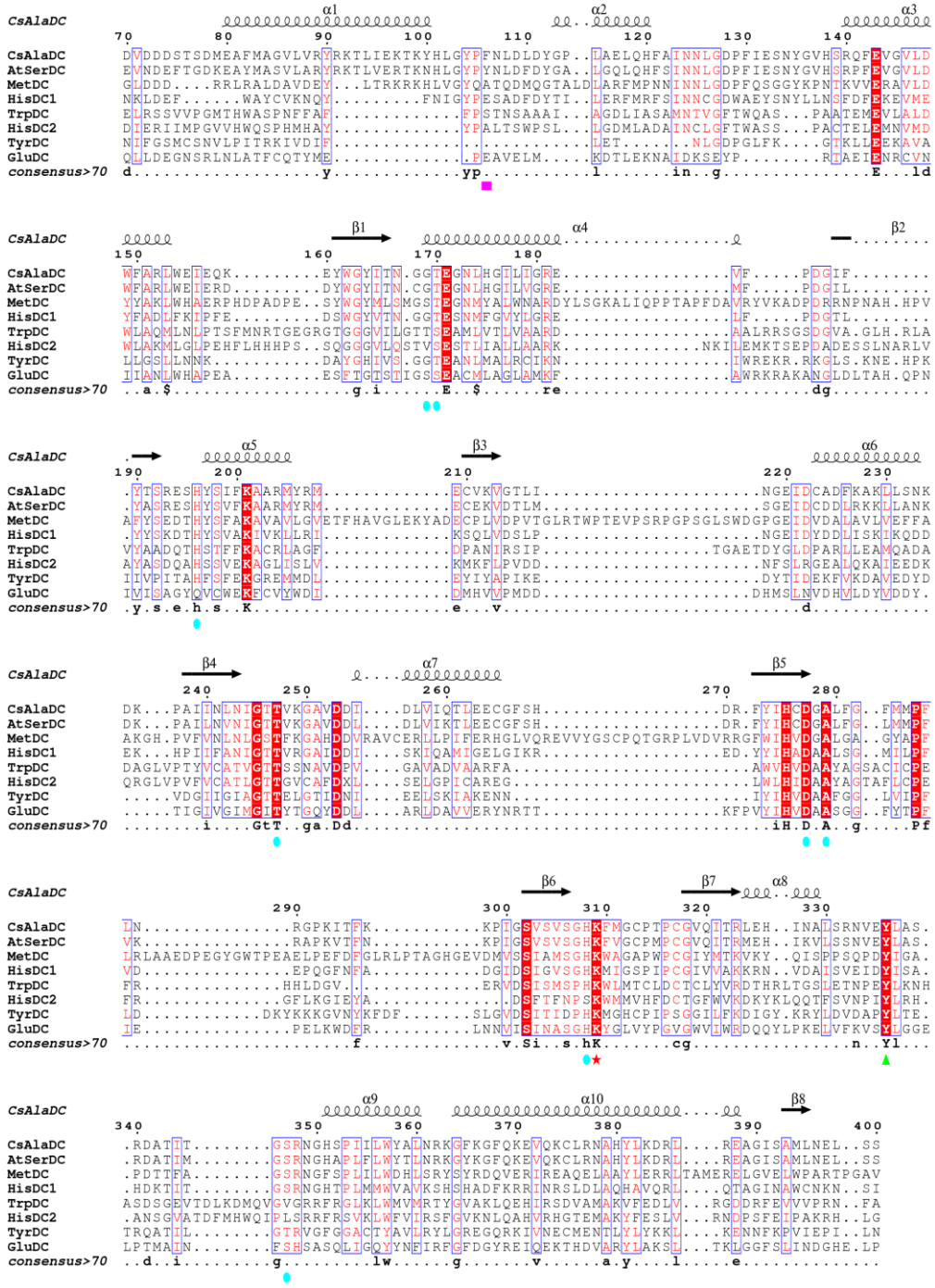

857

858 **Supplementary figure 5.** Multiple sequence alignment of CsAlaDC, AtSerDC, MetDC,

859 HisDC1, TrpDC, HisDC2, TyrDC, and GluDC were generated using MUSCLE and

visualized with ESPript 3.x. Conserved amino acid residues in all eight proteins are highlighted with red backgrounds. The magenta box marks key amino acid residues involved in substrate recognition for CsAlaDC and AtSerDC. The Lys residue covalently bound to the PLP cofactor is denoted by a red star, while the green triangle indicates the Tyr residue associated with enzymatic activity. Amino acid residues involved in the CsAlaDC substrate binding pocket are marked with blue circles.

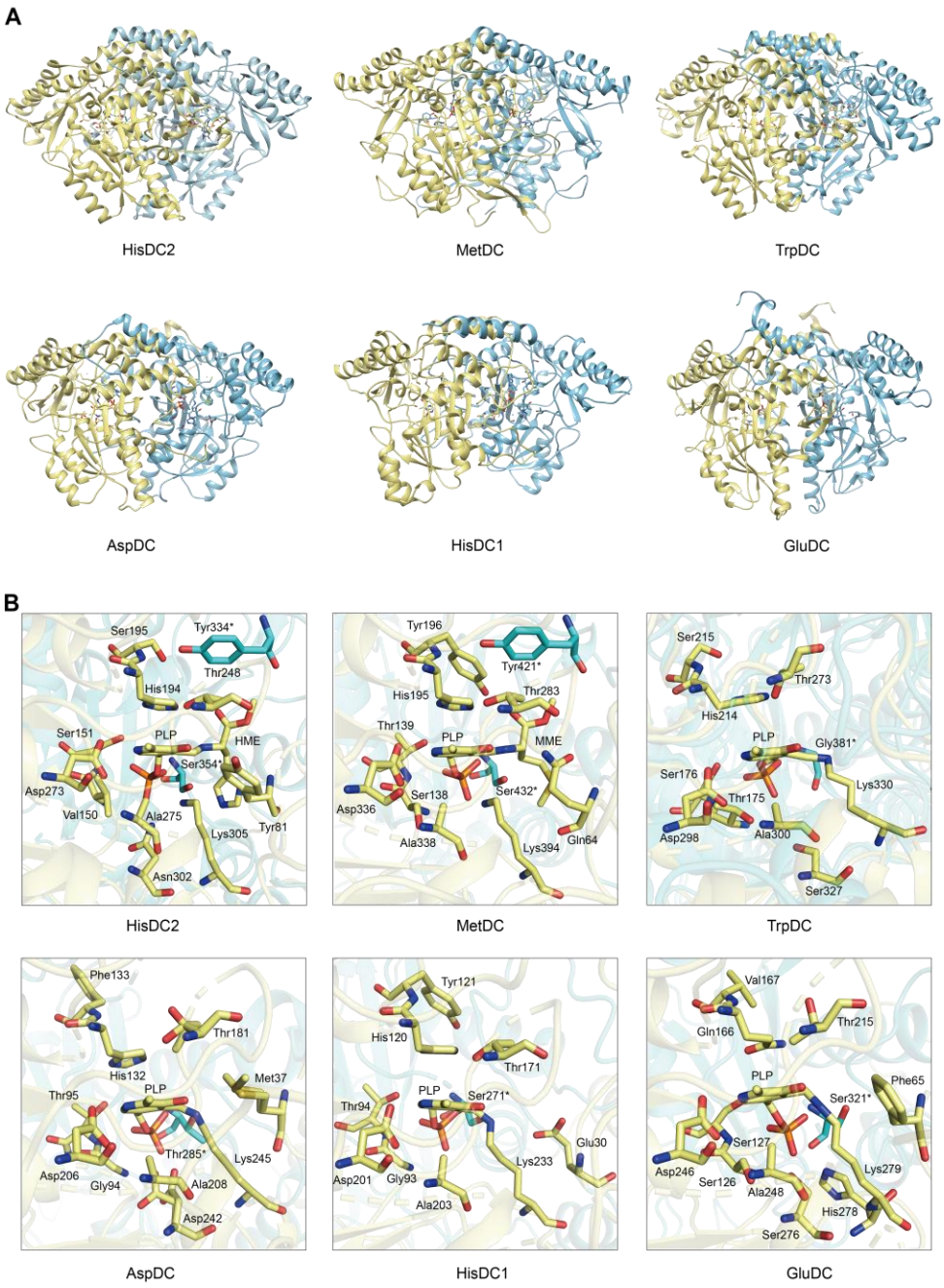

Supplementary figure 6. Structures of HisDC2, MetDC, TrpDC, AspDC, HisDC1 and GluDC. (**A**) The Overall Structures of HisDC2, MetDC, TryDC, AspDC, HisDC1 and GluDC. Chain A is shown in khaki, chain B is shown in cyan. (**B**) Amino acid residues in the substrate binding pocket of HisDC2, MetDC, TryDC, AspDC, HisDC1 and GluDC. The amino acid residues in chain A are shown in khaki, and the amino acid residues in chain B are shown in cyan.

Supplementary table 1. Amino acid sequence similarity matrix of the SerDC homologous protein

Accesion number	CsAlaDC	CsSerDC	PSS19488.1	PSS17472.1	XP_010108654.1	XP_027091704.1	XP_027148923.1	XP_007019463.1	XP_034676506.1	AtSerDC	XP_002266398.1	RVW94436.1	RVW37111.1	PWZ22363.1	PWZ25657.1	XP_008678685.1	NP_001403584.1	XP_015689218.1	XP_051217297.1	XP_047064312.1	KAF7016478.1	KAF7009155.1	GBG58923.1	XP_001689659.2	OAE25238.1	XP_024373856.1	XP_024371327.1	XP_002976233.2	XP_002987141.2
CsAlaDC	100	84.92	87.16	79.92	85.69	81.1	80.63	85.34	86.45	84.92	86.65	80.4	66.8	80.12	75.9	80.81	80.73	77.5	82.29	82.05	74.12	73.11	57.84	68.46	74.76	77.41	68.72	80.71	80.54
CsSerDC	84.92	100	86.04	78.03	87.02	86.14	85.07	88.1	90.12	86.21	89.92	84.44	69.69	83.56	77.43	82.34	84.99	81.2	83.2	82.79	76.56	76.51	58	66.54	76.53	78.63	71.05	80.97	81.26
PSS19488.1	87.16	86.04	100	87.5	89.12	88	87.48	88.26	90.53	86.86	90.53	85.05	69.29	85.86	79.69	84.9	86.13	84.76	86.67	86.25	78.84	79.51	61.27	69.06	72.01	79.22	67.83	82.3	82.3
PSS17472.1	79.92	78.03	87.5	100	80.45	78.6	77.73	80.16	81.99	79.38	81.99	76.99	75.54	74.9	72.61	76.12	76.12	72.44	77.48	76.86	71.67	72.35	53.73	67.01	67.22	73.35	64.84	75.82	75.98
XP_010108654.1	85.69	87.02	89.12	80.45	100	88.2	87.48	89.78	91.63	87.73	91.43	85.97	70.84	85.74	79.47	84.57	84.87	84.85	85.66	85.66	77.22	75.73	60.53	67.05	75.8	78.89	67.98	81.25	81.25
XP_027091704.1	81.1	86.14	88	78.6	88.2	100	99.4	88.29	88.4	86	88.65	82.14	74.5	85.29	78.33	82.32	82.97	84.72	82.24	81.15	73.45	81.4	64.38	67.83	76.69	79.81	71.71	81.51	81.71
XP_027148923.1	80.63	85.07	87.48	77.73	87.48	99.4	100	87.57	87.87	85.49	88.12	81.66	74.06	84.98	78.25	83.2	82.48	83.6	81.55	81.75	73.06	81.21	64.71	67.44	75.98	79.36	72.49	78.82	79.02
XP_007019463.1	85.34	88.1	88.26	80.16	89.78	88.29	87.57	100	91.65	87.9	91.45	84.72	70.96	85.1	77.49	82.35	85.14	79.89	85.57	85.37	77.7	81.54	58.29	68.15	79.66	78.9	71.4	82.29	82.09
XP_034676506.1	86.45	90.12	90.53	81.99	91.63	88.4	87.87	91.65	100	87.12	99.59	92.53	77.18	84.33	78.24	82.27	84.62	84.79	85.19	85.19	78.46	78.61	60.33	66.73	74.21	79.92	72.89	83.57	83.16
AtSerDC	84.92	86.21	86.86	79.38	87.73	86	85.49	87.9	87.12	100	87.65	81.26	67.95	82.24	77.07	82	85.51	79	83.71	83.88	78.87	81	61.02	66.34	72.63	77.42	69.6	80.98	81.02
XP_002266398.1	86.65	89.92	90.53	81.99	91.43	88.65	88.12	91.45	99.59	87.65	100	92.93	76.98	83.43	77.34	82.27	84.41	84.79	84.66	85.04	77.7	78.61	60.16	66.73	77.06	78.1	72.89	83.37	82.96
RVW94436.1	80.4	83.17	83.77	76.99	85.97	82.14	81.66	84.72	92.53	81.26	92.93	100	70.79	77.12	71.48	75.92	77.91	78.26	79.52	79.88	73.08	73.94	56.41	62.12	72.37	72.12	68.14	76.8	76.4
RVW37111.1	66.8	69.69	69.29	75.54	70.84	74.5	74.06	70.96	77.18	67.95	76.98	70.79	100	64.64	62.87	65.89	64.73	64.85	68.27	68.27	60.07	60.36	46.62	53.3	59.67	65.35	59.58	65.03	64.64
PWZ22363.1	80.12	83.56	85.86	74.9	85.74	85.29	84.98	85.1	84.33	82.24	83.43	77.12	64.64	100	89.35	95.14	90.71	90.02	87.88	87.88	78.73	79.05	61.86	70.3	76.65	79.35	71.98	80.72	80.64
PWZ25657.1	75.9	77.43	79.69	72.61	79.47	78.33	78.25	77.49	78.24	77.07	77.34	71.48	62.87	89.35	100	93.86	83.78	82.96	82.38	82.38	78.74	77.9	64.32	64.09	71.53	72.92	64.33	76.23	76.04
XP_008678685.1	80.81	82.34	84.9	76.12	84.57	82.32	83.2	82.35	82.27	82	82.27	75.92	65.89	95.14	93.86	100	89.23	88.25	87.76	87.76	78.35	78.86	60.36	68.1	75.85	77.39	67.87	81.12	80.92
NP_001403584.1	80.73	84.99	86.13	76.12	84.87	82.97	82.48	85.14	84.62	85.51	84.44	79.17	64.73	90.71	83.78	89.23	100	92.54	88.8	88.8	79.52	79.66	62.61	69.11	75.75	77.46	72.4	82.24	82.04
XP_015689218.1	77.65	81.2	84.76	72.44	84.85	83.69	83.6	79.89	84.79	79	84.79	79.48	64.85	90.02	82.96	88.25	92.54	100	87.17	87.12	78.39	78.35	61.49	69.57	73.46	72.08	68.5	79.28	79.28
XP_051217297.1	82.29	83.2	86.67	77.48	85.66	82.24	81.55	85.57	85.19	83.71	84.66	79.52	68.27	87.88	82.38	87.76	88.8	87.17	100	98.93	83.4	83.37	61.56	68.39	73.67	76.86	67.88	82.24	82.04
XP_047064312.1	82.05	82.79	86.25	76.86	85.66	81.15	81.75	85.37	85.19	83.88	85.04	79.88	68.27	87.88	82.38	87.76	88.8	87.12	98.93	100	83.02	82.79	60.93	63.81	72.52	77.46	68.06	82.55	82.34
KAF7016478.1	74.12	76.56	78.84	71.67	77.22	73.45	73.06	77.7	78.46	78.87	77.7	73.08	60.07	78.73	78.74	78.35	79.52	78.39	83.4	83.02	100	90.69	63.88	63.47	69.5	70.6	69.4	75.7	75.51
KAF7009155.1	73.11	80.46	79.51	72.35	75.73	81.4	81.21	81.54	78.61	81	78.61	73.94	60.36	79.05	77.9	78.86	79.66	78.35	83.37	82.79	90.69	100	63.5	64.29	69.91	70.9	68.02	75.46	75.28
GBG58923.1	57.84	58	61.27	53.73	60.53	64.38	63.46	58.29	60.33	61.02	60.16	56.41	46.62	61.86	64.32	60.36	62.61	61.49	61.56	60.93	63.98	63.5	100	53.95	62.46	66.1	64.11	61.98	62.63
XP_001689659.2	68.46	66.6	69.06	67.01	67.05	67.57	67.18	68.15	66.73	66.34	66.73	62.12	53.3	70.3	64.09	68.1	69.11	69.57	68.39	63.81	63.47	64.29	53.95	100	67.92	65.79	61.89	70.56	70.16
OAE25238.1	74.76	76.53	72.01	67.22	75.8	76.69	75.98	79.66	74.21	72.63	77.06	72.37	59.67	76.65	71.53	75.85	75.75	73.46	73.67	72.52	69.5	69.91	62.66	67.92	100	83.21	75.17	79.92	79.73
XP_024373856.1	77.41	78.63	79.22	73.35	78.89	79.81	79.36	78.9	79.92	77.42	78.1	72.12	65.35	79.35	72.92	77.39	77.46	72.08	76.86	77.46	70.6	70.9	66.1	65.79	83.21	100	81.15	78.46	78.27
XP_024371327.1	68.72	71.05	67.83	64.84	67.98	71.71	70.69	71.4	72.89	69.6	72.89	68.14	59.58	71.98	64.33	67.87	72.4	68.5	67.88	68.06	69.4	68.02	64.47	61.89	75.17	81.15	100	72.53	72.53
XP_002976233.2	80.71	80.97	82.3	75.82	81.25	81.51	78.82	82.29	83.57	80.98	83.37	78.02	65.03	80.72	76.23	81.12	82.24	79.28	82.24	82.55	75.7	75.46	61.98	70.56	79.92	78.46	72.53	100	99.79
XP_002987141.2	80.54	81.26	82.3	75.98	81.25	81.71	79.02	82.09	83.16	81.02	82.96	77.62	64.64	80.64	76.04	80.92	82.04	79.28	82.04	82.34	75.51	75.28	62.63	70.16	79.73	78.27	72.53	99.79	100

877 **Supplementary table 2**. Data collection and refinement statistics

	CsAlaDC	CsAlaDC-EA complex	AtSerDC
Data Collection			
Space Group	*P3121*	*P3121*	*C2*
Cell Dimensions			
a, b, c (Å)	163.5,163.5, 50.2	164.0,164.0,50.2	115.4,149.5,139.1
α, β, γ (°)	α=β=90, γ=120	α=β=90, γ=120	α=γ=90, β=109.2
Wavelength (Å)	0.979	0.979	0.979
Resolution (Å)	50-2.50	50-2.60	50-2.85
Completeness (%)	99.3 (99.9)	99.6 (100.0)	99.6 (98.1)
Redundancy	5.4 (5.1)	13.0 (12.5)	5.9 (5.0)
$<I>/<\sigma I>$	9.3 (1.9)	18.9 (4.6)	10.6 (2)
R_{merge}	0.128 (0.603)	0.156 (0.562)	0.173 (0.551)
Refinement			
R_{work}/ R_{free}	0.173/0.222	0.172/0.223	0.214/0.262
No. reflections	25175	22813	49543
B-facator (Å^2)			
Protein	43.3	48.3	57.6
PLP	29.5	31.5	52.8
Zn^{2+}	58.7	43.8	71.6
Ca^{2+}	-	55.5	-
Ethylamine	-	27.5	-
Glycerol	-	-	51.7
Water	38.5	40.9	-
R.m.s. deviations			
Bond lengths (Å)	0.008	0.008	0.007
Bond angles (°)	1.531	1.601	1.410
No. of atoms			
Protein	3292	3265	3250
PLP	15	15	60
Zn^{2+}	2	1	4
Ca^{2+}	-	1	-
Ethylamine	-	5	-
Glycerol	-	-	24
Water	115	60	-
Ramachandran statistics (%)			
Favoured	94.01	93.58	91.52
Allowed	5.74	5.68	7.61
Outliers	0.25	0.74	0.87

878 R_{merge}=∑hkl∑i|Ii(hkl)-<I(hkl)>|/∑hkl∑i Ii(hkl), where<I(hkl)>is the main value of I(hkl).

879 R_{work}=∑||Fobs|-|Fcalc||/∑|Fobs|, where Fobs and Fcalc are observed and calculated structure
880 factors.

881 The free R factor was calculated using 5% of reflections ommitted from the refinement.

882 Highest resolution shell is shown in parenthesis

Supplementary table 3. Primers used for gene cloning.

Name	Forward primers (5'-3')	Reverse primers (5'-3')
CsAlaDC	GGAATTCCATATGACAACAAGCCTCACCATCACGG	GATCTCGAGTCATTTATGAAGATCACAATCACAATTCTCACTTC
AtSerDC	GGAATTCCATATGACCACCAGCCTGGCCG	GATCTCGAGTTATTTATGGGCCGGACAAATGCAATTATTG
CsSerDC	ATGGTGGGAAGTGTTGGGGT	TCACTTGTGTAGTGCACAAAGACAGT

Supplementary table 4. Primers used for real-time PCR.

Name	Forward primers (5'-3')	Reverse primers (5'-3')
CsAlaDC	CACTGTGATGGGGCTCTGTT	TGTTATCTGGACACCGCACG
AtSerDC	TCACTCGCTGTAACGGAACC	AACTGACCAAGCGCACCATA
NbGAPDH	AGCTCAAGGGAATTCTCGATG	AACCTTAACCATGTCATCTCCC